R E P O R T

on the subject " Growth and Characterization of Bulk Silicon Carbide for Electronics , Microwave Applications and Optical Application "
SPC - 94 - 4085

KIEV , UKRAINE

1995

REPORT DOCUMENTATION PAGE

Form Approved OMB No. 0704-0188

1. AGENCY USE ONLY (Leave blank)	2. REPORT DATE	3. REPORT TYPE AND DATES COVERED
	1995	Final Report

4. TITLE AND SUBTITLE

Growth and Characterization of Bulk Silicon Carbide for Electronics, Microwave Applications, and Optical Applications

5. FUNDING NUMBERS

F6170894W0770

6. AUTHOR(S)

Dr. Felix Nazarenkov

7. PERFORMING ORGANIZATION NAME(S) AND ADDRESS(ES)

Academy of Sciences of the Ukraine
Special Design Technology
Lisogorskaya St 4
Kiev 252028
Ukraine

8. PERFORMING ORGANIZATION REPORT NUMBER

N/A

9. SPONSORING/MONITORING AGENCY NAME(S) AND ADDRESS(ES)

EOARD
PSC 802 BOX 14
FPO 09499-0200

10. SPONSORING/MONITORING AGENCY REPORT NUMBER

SPC 94-4085

11. SUPPLEMENTARY NOTES

12a. DISTRIBUTION/AVAILABILITY STATEMENT

Approved for public release; distribution is unlimited.

12b. DISTRIBUTION CODE

A

13. ABSTRACT (Maximum 200 words)

This report results from a contract tasking Academy of Sciences of the Ukraine as follows: Grow both 6H and 15R SiC using the Lely growth technique or other appropriate techniques as described in the attached proposal dated 22 July 1994. The SiC will be characterized by structural, physical and chemical analysis.

14. SUBJECT TERMS

EOARD

15. NUMBER OF PAGES

73

16. PRICE CODE

N/A

17. SECURITY CLASSIFICATION OF REPORT	18. SECURITY CLASSIFICATION OF THIS PAGE	19. SECURITY CLASSIFICATION OF ABSTRACT	20. LIMITATION OF ABSTRACT
UNCLASSIFIED	UNCLASSIFIED	UNCLASSIFIED	UL

C O N T E N T S

INTRODUCTION 3

SECTION I .Growth and investigation of silicon carbide parameters fabricated by the sublimation method 3

1.1.Growth of SiC single- crystals.The technique and equipment 5

1.2.Polycrystalline SiC.The technique and equipment 6

1.3.Parameters of the polycrystalline SiC 9

1.4.Investigation of single-crystal parameters 11

1.4.1.Analysis of impurity composition 11

1.4.2.Investigation of structural perfection 12

1.4.3.Identification of SiC-polytypes by the Raman Scattering and X-ray diffractometric methods 22

1.4.4.Spectrum of nitrogen in 6H and 15R SiC 27

1.4.5.Surface electron properties of the 6H and 15R modification silicon carbide 35

SECTION II.AVALANCHE LIGHT EMITTING DIODES

2.1.Investigation of parameters and technology 51

2.2.Technical parameters 60

SECTION III.HIGH-TEMPERATURE THERMAL RESISTORS BASED ON SILICON CARBIDE

3.1.Thermal resistors based on the polycrystalline SiC 62

3.2.Thermal resistors based on bulk crystals of SiC 64

REFERENCES 70

INTRODUCTION

Silicon carbide is the only binary compound of carbon and silicon existing in a solid phase. It crystallizes in either the sphalerite (β-SiC or 3C-SiC) or wurtzite (α-SiC) structure with formation of ion-covalent bonds. A high Si-C bond energy in silicon carbide (~5 eV) provides its resistance to high temperature and radiation, imparts mechanical strength and chemical stability and causes low diffusion coefficients of dopants and host atoms. Among the materials, which impurity conduction of both the n- and p-type can be controlled within wide limits, SiC is distinguished as possessing the widest band gap, which ranges from 2.3 eV for the cubic polytype 3C-SiC up to 3.4 eV for the hexagonal polytype 2H-SiC. Silicon carbide has also a high saturated electron drift velocity which improves performances of devices destined to operate at high speed, high power levels. Its high thermal conductivity permits high-density device integration.

A number of techniques for growth of silicon carbide crystals has been proposed by different researchers. These techniques in general can be sorted over three broad classes. Yet, it seems to be not so easy to carry out this classification according such a scheme. The first technique is known as the method of chemical deposition in reagent gases introduced in a system within which they form the SiC crystals on an appropriate substrate. The second technique consists in crystallization from the silicon melt. The last type of main techniques for growth of SiC crystals is usually referred to as the sublimation method.

1 SECTION

GROWTH AND INVESTIGATION OF SILICON CARBIDE PARAMETERS FABRICATED BY THE SUBLIMATION METHOD

The most successful synthesis of SiC has been performed by the sublimation method. The earliest technological procedure for preparation of SiC is the so-called Acheson process. This method

is used for commercial production of SiC. It consists in that a mixture of silicon and carbide is heated up to 2500 - 2700 ^{o}C. The reaction yield is mainly the 6H-modification polycrystalline material. In some hollow cavities the single-crystal plates with the outline size up to 10 to 20 mm are formed. The crystals fabricated by this method cannot be used as substrates for semiconductor devices because the crystals grown are too small. The main shortcoming in the method consists in that one cannot control the process of nucleation, that leads to a large scatter of structural and electrophysical properties resulting in a low yield of suitable crystals.

Another sublimation procedure, which is virtually much better controlled, is the Lely method [1]. This method consists in vaporization of a SiC charge at about 2500 ^{o}C.Into a cooler cavity with subsequent condensation. Initially the charge forms its own cavity, while the more uniform crystals grow when a thin graphite cylinder is placed in the center of the charge. Such a thin cylinder reduces also a number of nucleation centers so that fewer and more perfect crystals grow. The crystals grow as thin hexagonal platelets perpendicular to the growth cavity surface. The 6H modification prevails among these crystals while other modifications such as 15R, 8H and 21R are found as well.

Tairov [2-4] has developed the method of fabrication of the 6H-SiC single-crystal ingots with using seed crystals by employing the modified Lely method in vacuum. When using this method, the crystal ingots with up to 20 mm diameter were obtained by Ziegler et al. [5,6] and the inch-size crystals of 6H-SiC were obtained by K.Koga, Nakata et al. [7-9]. These authors made use of various polytype seed crystals with the (0001) basal planes or the planes deviating by a few degrees from (0001). The crystal growth was carried out at temperatures around 1800 ^{o}C under the vacuum 10^{-3} to 10^{-4} bar with the axial temperature gradient in the growth zone of 30 to 40 ^{o}C/cm. Tairov and Tsvetkov [4] stated that using seed crystals with a given polytype is a reliable method for growing ingots of a desired polytype. On the other hand, they

marked problems as to preventing simultaneous growth of several polytype modifications in a single-crystal.

1.1. Growth of SiC single-crystals. The technique and equipment.

The SiC crystals have been grown in the special vertical-type high-temperature furnaces (Редмет-30) made of stainless steel and with water-cooled walls. High temperatures were provided with a heater consisting of a cylindrical graphite tube having a complicated form to provide a required temperature field in the growth zone. The equilibrium conditions in the growth zone to provide a homogeneous deposition take place usually in the closed systems because in such systems a material removal from a container space through a vapor phase is absent. Unfortunately, it is difficult to make an entirely closed system for growing SiC because of absence of a suitable container material. The vacuum-tight graphite container with a thin graphite cylinder placed in the container center has been used for our growth process. The SiC powder as a source material is loaded between the container walls and the graphite cylinder. When heated, the SiC powder evaporates and due to a presence of a temperature gradient it diffuses through pores in the graphite cylinder and then condenses on the walls.One can write the following set of chemical reactions for the Si-C system:

$$SiC_{sol} \rightleftarrows SiC_{gas}$$
$$SiC_{sol} \rightleftarrows 1/2\ Si_2C_{gas} + 1/2\ C_{sol}$$
$$SiC_{sol} \rightleftarrows 1/2\ SiC_{2\ gas} + 1/2\ Si_{gas,liq}$$
$$SiC_{sol} \rightleftarrows Si_{gas,liq} + C_{sol}$$

We have used the commercial-grade SiC as a source material. Secondly, we have used SiC synthetized at our laboratory.The growth process was carried out within the temperature range 2200 to 2400 ^{o}C at the partial pressure of an inert gas (Ar or He) from 10^{-5} to 10^{-1} torr. The temperature was measured using an optical pyrometer in several parts of the growth zone.

The process duration ranged from 5 to 12 h.

The doping level of SiC crystals depends strongly on the impurity composition of an initial material, the inert gas purity and quality of the graphite units as well as on the outgassing cycle duration.

Fig.1.1 illustrates a cross-sectional view of the sublimation crucible.

1.2. Polycrystalline SiC. The technique and equipment.

To grow polycrystalline SiC we have used the method of synthesis from the Si an C separate sources. This method uses vaporization of Si from a graphite container with a subsequent condensation of SiC on a graphite lid. A large amount of superpure graphite used for a crucible and other units of the high-temperature furnace is indicative of this apparatus. Graphite units in the system represent a reservoir of carbon. The following set of chemical reactions can be written in this case:

$$Si_{liq,gas} + C_{sol} \rightleftarrows SiC_{gas}$$
$$2Si_{liq,gas} + C_{sol} \rightleftarrows Si_2C_{gas}$$
$$Si_{liq,gas} + 2C_{sol} \rightleftarrows SiC_2\ gas$$

The synthesis was carried out at 1800 to 2000^{0}C under the vacuum 10^{-4} to 10^{-2} torr. The growth rate depends on the temperature of growth and achieves 0.2 to 2 mm/h.

It is possible to obtain layers which are up to 10 mm thick [10]. Formed as a rule at synthesis temperatures T<=1800^0 C is the 3C-SiC modification. Temperature increasing leads to formation of α-SiC. The structure of layers depends on the deposition rate. Dense layers are formed at the maximum deposition rate. A grain growth direction in regard to a substrate is determined by directions of vapor fluxes. The maximum cross-section size of the grains is 250 to 500 μm.

After SiC growth a graphite substrate was removed by burning in air at 750 to 900 ^{0}C.

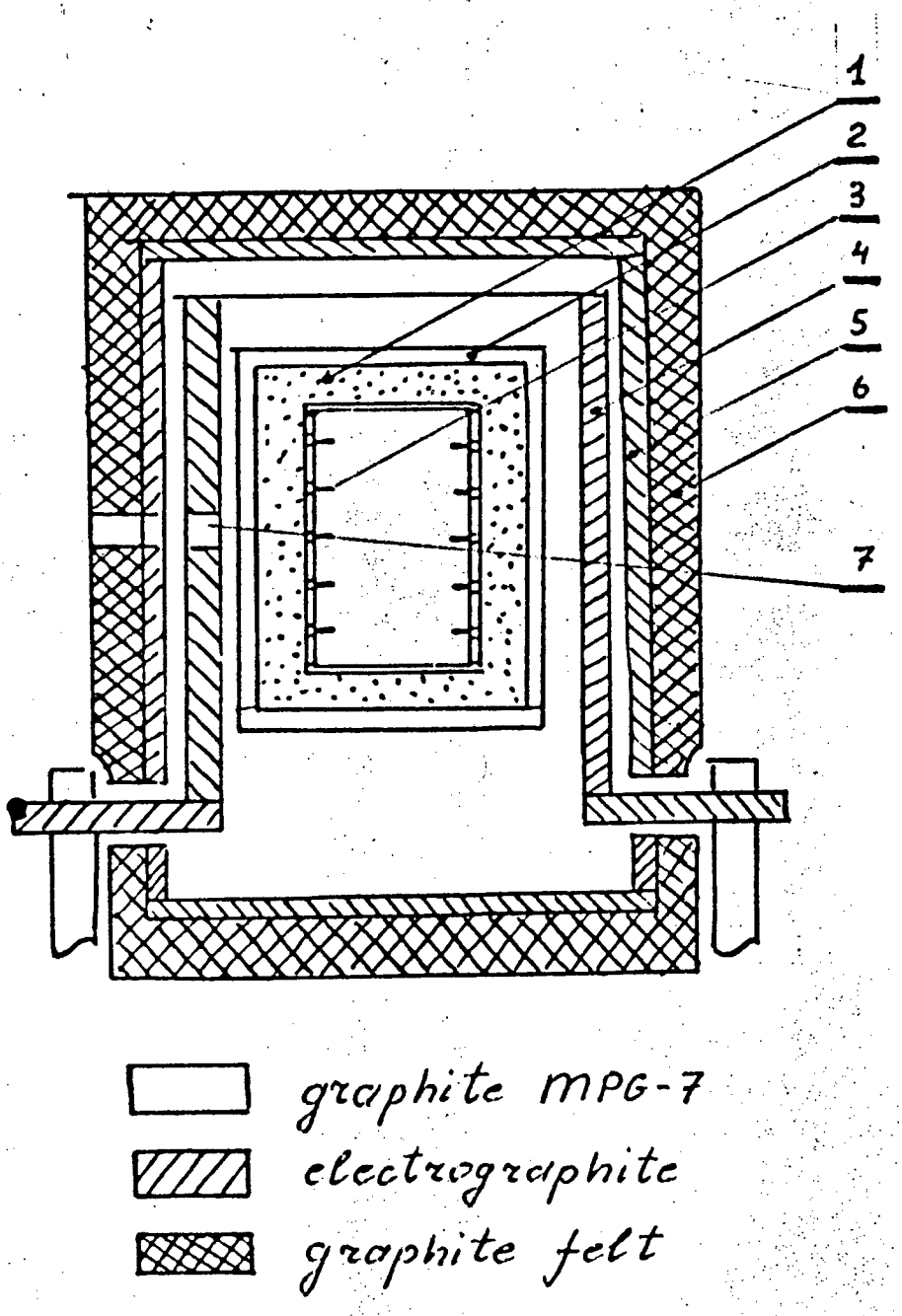

Fig. 1.1. Cross-sectional view of the sublimation crucible : 1 - SiC powder ; 2 - crucible ; 3 - fabricated crystal ; 4 - heater ; 5 - heat shield ; 6 - heat-insulating material ; 7 - pyrometer opening .

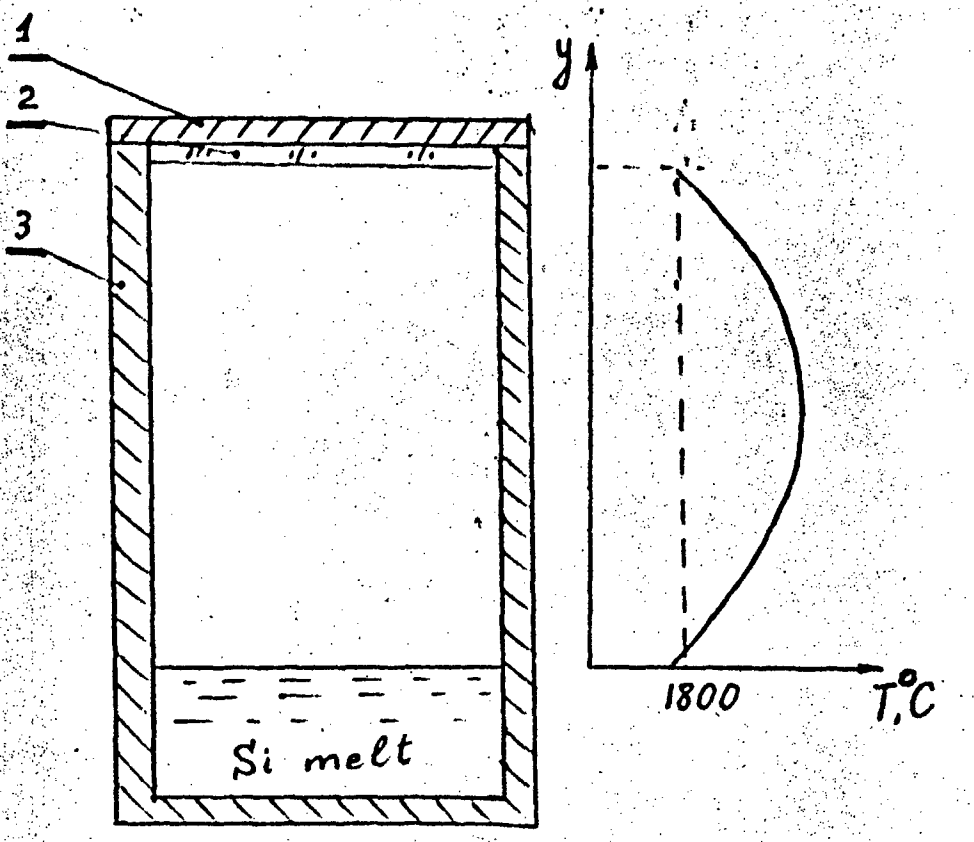

Fig. 1.2. Scheme of the crucible for the growth of polycrystalline SiC .

Fig.1.2 shows the set-up arrangement.

1.3. Parameters of the polycrystalline SiC

The resistivity of the SiC material synthetized under different conditions may range within the limits ρ=2.5 to 400 Ohm cm. According to the data of a spectral analysis the percentage content of main impurities is as follows:

Element percentage

Element	Specimen	
	No.1	No2
Ca	10^{-3} to 10^{-5}	-
Cu	-	$3*10^{-4}$
Fe	10^{-3} to 10^{-4}	$3*10^{-4}$
Al	10^{-2}	$<3*10^{-3}$
Mg	10^{-3} to 10^{-4}	10^{-3}
Sb	-	-
Ti	10^{-5}	-
B	-	-
p	-	-

Fig.1.3 presents the results of measuring the Hall effect for the sample with the resistivity ρ=270 Ohm cm. It is seen that the electron concentration increases with temperature almost exponentially over the range 80 to 300 K within the limits $2.9*10^{15}$ to $4*10^{17}$ cm^{-3}. The mobility μ_n within the range 100 to 300 K is nearly constant and equal to 0.15 cm^2/V s. Only at temperatures near to 80 K its value somewhat increases, remaining

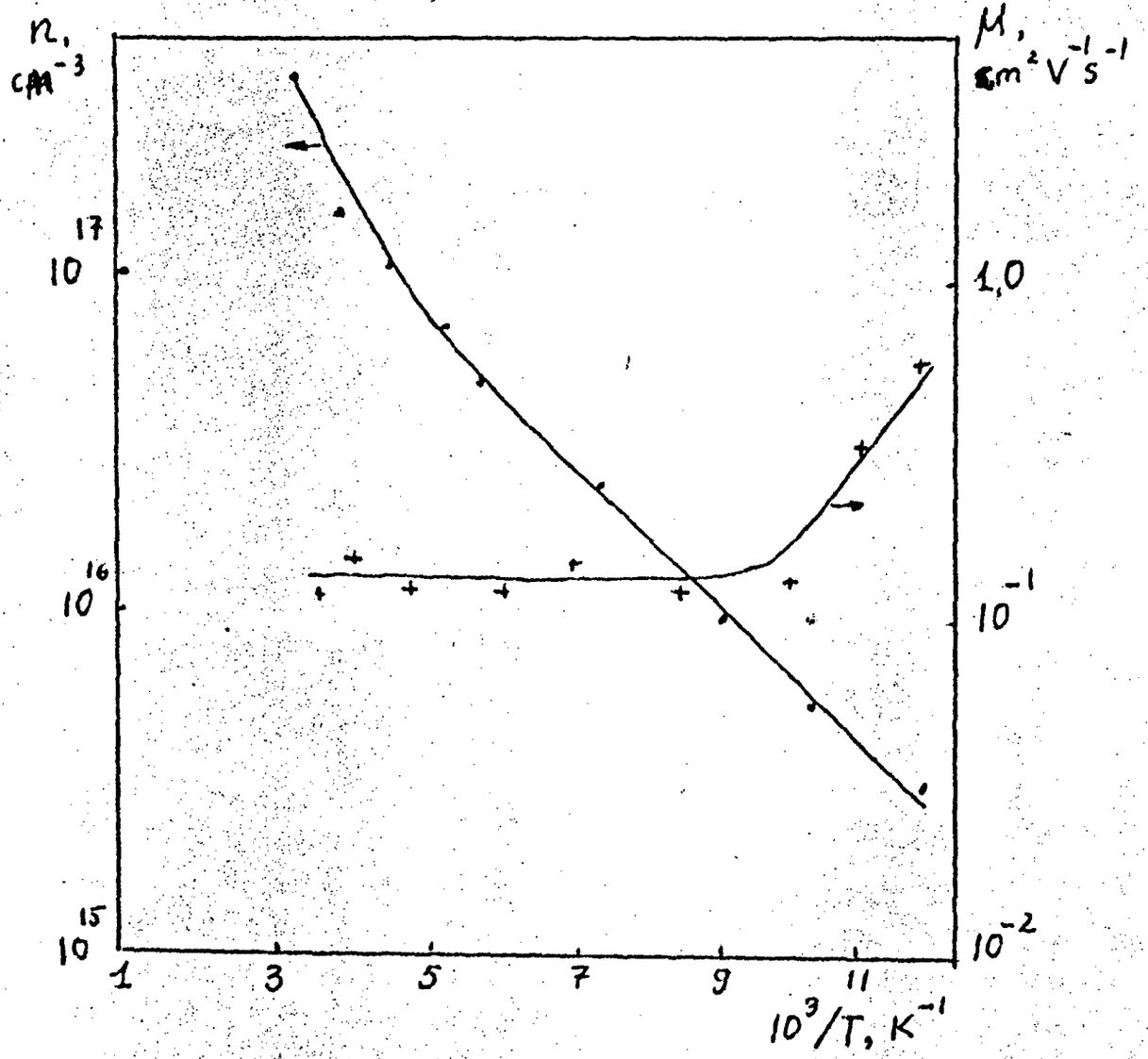

Fig. 1.3. Temperature dependences of concentration and mobility of polycrystalline SiC .

less than 1.0 $cm^2/V \cdot s$. The activation energy calculated from a slope of the n=f(1/T) dependence is 0.04 eV, which corresponds to the energetic position of nitrogen in regard to the c-band of 3C-SiC. Thus, one may assume that the electron concentration in our samples is determined by ionized levels of nitrogen the concentration of which is (3 to 8)$\cdot 10^{17}$ cm^{-3}.

We suppose that the presence of boundaries between micrograins of 3C-SiC gives insignificant effect on a measured value of the Hall coefficient and an electron concentration determined from it. This is caused by the fact that the micrograin dimensions are by three orders of magnitude larger than the free path of electrons in the case of scattering by impurities at impurity concentrations ~10^{18} cm^{-3}. On the other hand, the presence of intercrystal boundaries significantly decreases the efficient electron mobility in the samples under study. Therefore, the mobility values for polycrystalline samples are by three orders of magnitude less than that for the 3C-SiC single crystal. Invariability of a measured efficient mobility over the range 100 to 300 K is caused by a constant value of energetic barriers at microcrystal boundaries [10].

1.4. Investigation of single-crystal parameters.

1.4.1. Analysis of impurity composition

We have used the X-ray microprobe analyzer being a part of the scanning electron microscope JOEL (Japan), the JAM845 Model, with an auxiliary unit for microprobe analysis (Link-system). This technique is destined for a sample composition analysis with a depth of analysis dependent on the accelerating voltage of an electron microprobe (5 to 50 kV) and atomic numbers of materials under study. The analysis depth is within the limits 0.2 to 1.5 μm. The method is based on the fact that the line intensity of the characteristic X-rays is proportional to percentage of a given element in a sample. The method enables to analyze elements with atomic numbers from 6 to 100 and has the sensitivity of 0.5 %wt. The characteristic emission is received by the detector with

energetic dispersion, the AN10000 type, trough special windows. For light elements with small emission energy one uses a thin window, while for heavy elements the thicker beryllium window is applied. To remove a charge from dielectrics, a thin gold film (~50 Å) is deposited on a surface which because of its small thickness does not manifest itself in a spectral pattern. Three typical samples have been analyzed: No.1 - 15R, No.2,.3 - 6H-SiC. As following from the spectral patterns(Fig.1.4-1.9), all the samples have the same element composition in regard to impurity contents. The samples are homogeneous by both their depth and surface area. Present in the samples under study are oxygen and phosphorus at a trace level (no more than 1 %wt). One observes such impurities as Na, S, Cl, K.

1.4.2. Investigation of structural perfection

This investigation has been carried out for the 6H- and 15R-SiC single-crystal plates cut perpendicular to the c axis. The plates were polished with diamond pastes and then etched for 2 min in the $KOH-KNO_3$ (1:4) melt at 650°C.

The Lang projection method [11] and the transmission hold-frame method [12] have been used as X-ray topographic methods with employing the $MoK_{\alpha 1}$ emission and the $\{\bar{1}120\}$, $\{\bar{3}300\}$, $\{\bar{1}011\}$ reflexes which possess the largest reflectivity. Chosen for studies were the samples with well developed pyramidal $\{1\bar{0}11\}$ faces and the (0001) face being a base of a pyramid. Such crystals are more perfect.

The most frequently used to obtain projection topographic patterns are the $\{\bar{1}120\}$-like reflexes since they are more informative. The reflexes like $\{\bar{3}300\}$ and $\{1\bar{0}11\}$ were used to determine the Burgers vector directions in separate plane clusters of dislocations from "extinguishing" their reflexes [13].

One should remove a damaged surface layer formed after mechanical processing. For this purpose we used chemical etching. A surface damaged layer consists of individual scratches creating elastic deformations which spread into a large depth. Presented in

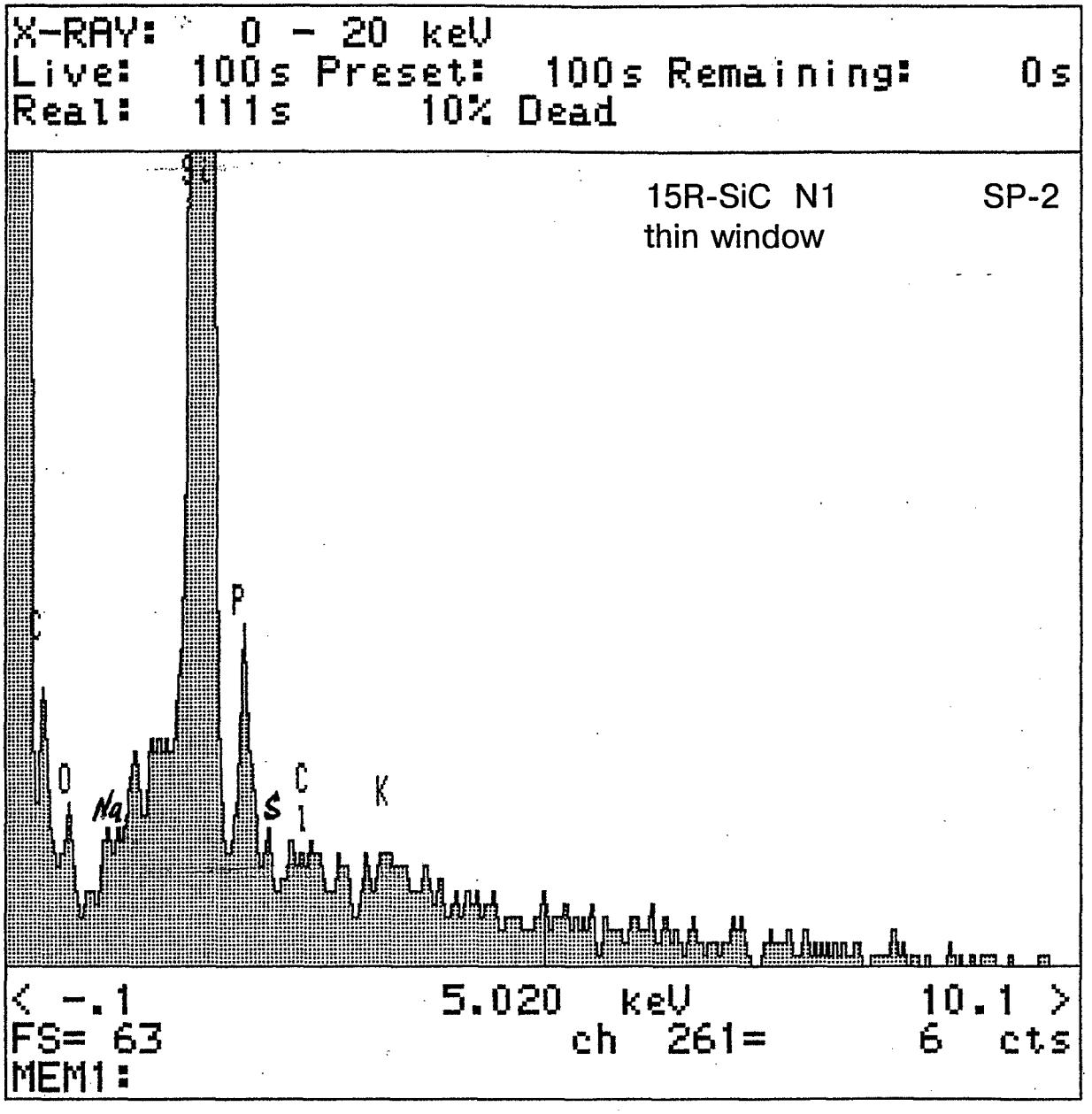
X-RAY: 0 - 20 keV
Live: 100s Preset: 100s Remaining: 0s
Real: 111s 10% Dead
15R-SiC N1
thin window
SP-2
C
O
Na
P
S
Cl
K
< -.1
5.020 keV
10.1 >
FS= 63
ch 261= 6 cts
MEM1:

Fig 1.4.

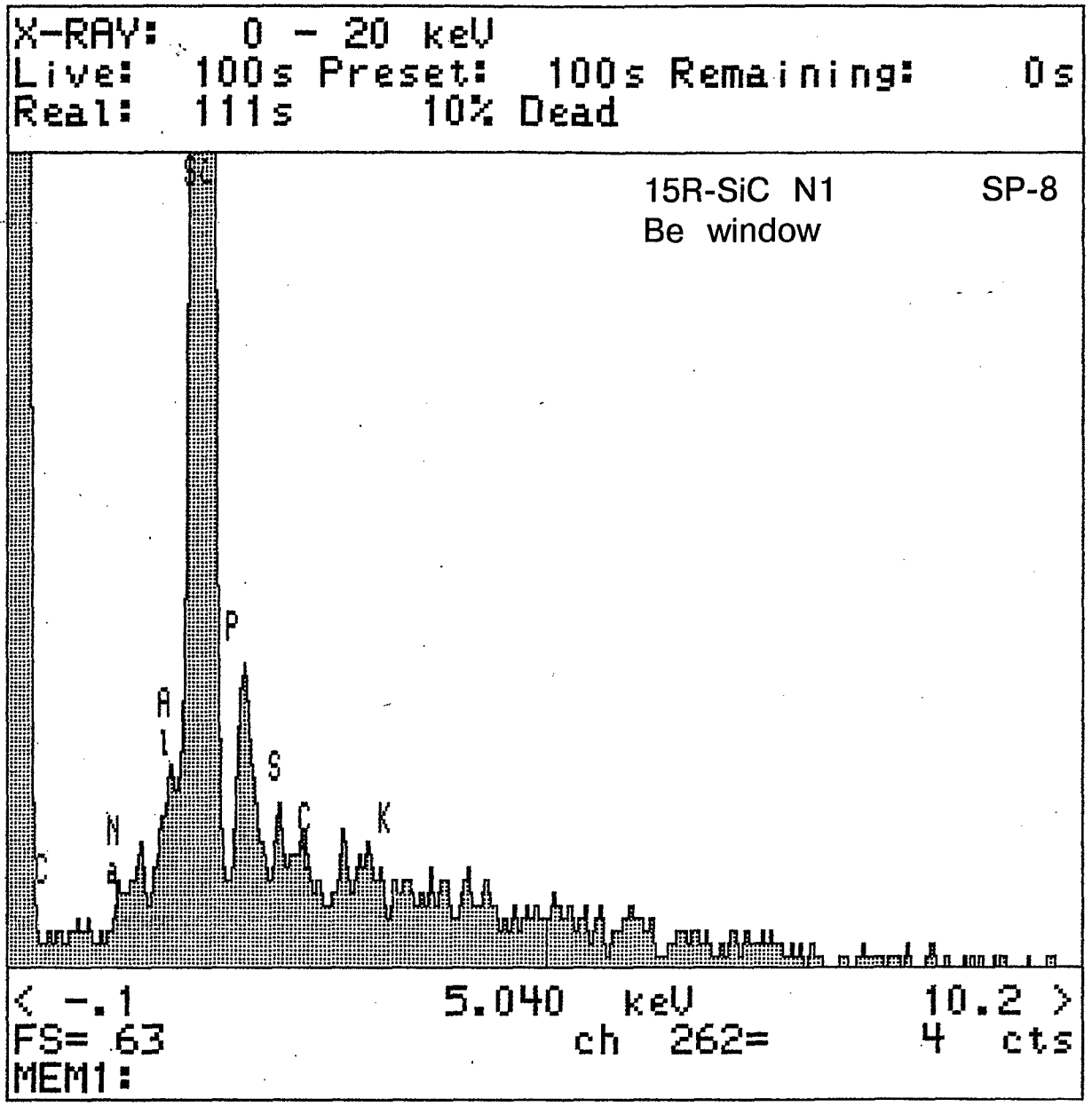
X-RAY: 0 - 20 keV
Live: 100s Preset: 100s Remaining: 0s
Real: 111s 10% Dead
15R-SiC N1 SP-8
Be window
Si
P
A
L
S
C
K
N
C
< -.1
5.040 keV
10.2 >
FS= 63
ch 262= 4 cts
MEM1:

Fig 1.5.

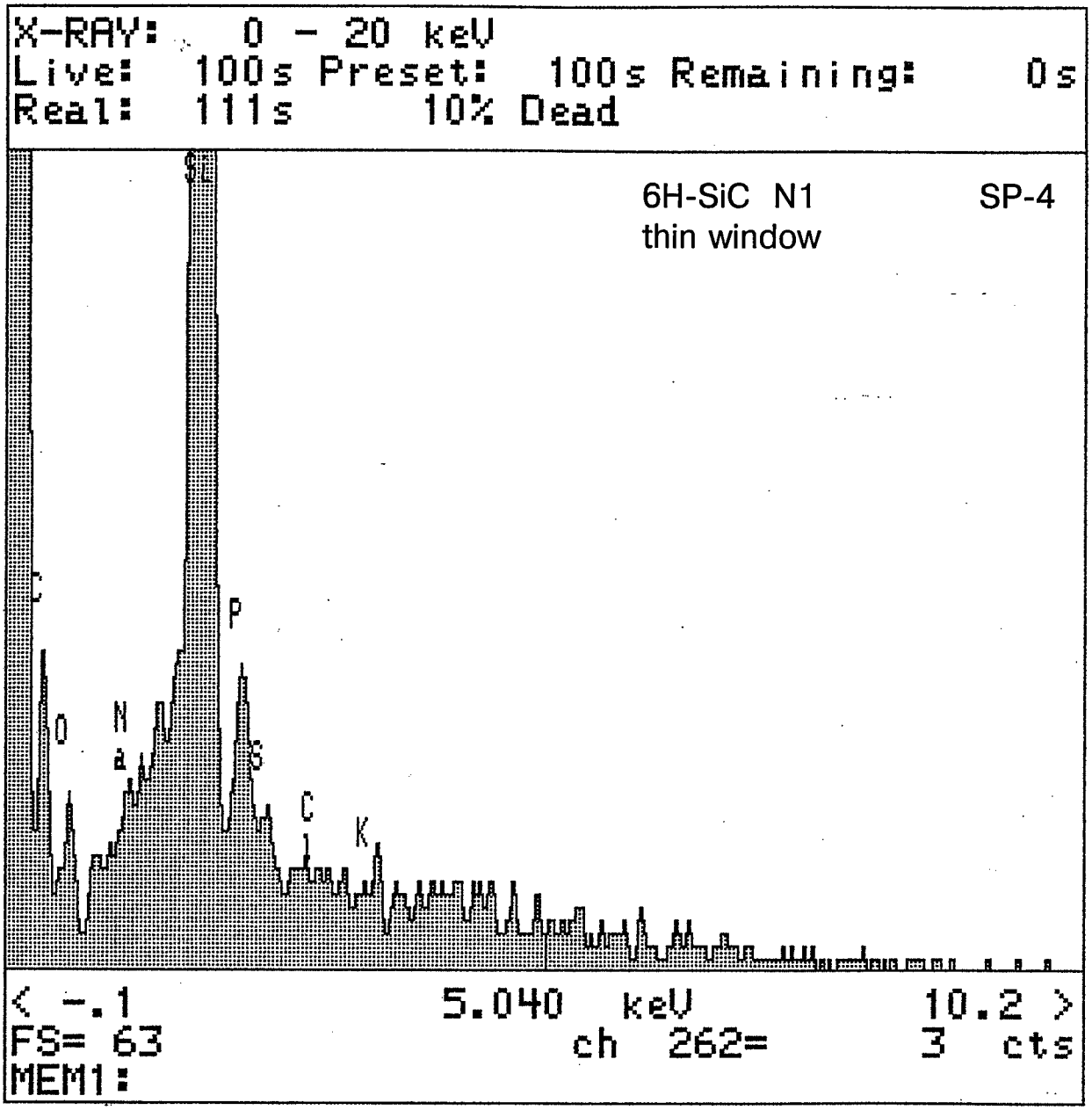
X-RAY: 0 - 20 keV
Live: 100s Preset: 100s Remaining: 0s
Real: 111s 10% Dead
6H-SiC N1
thin window
SP-4
Si
P
O
Na
S
Cl
K
< -.1
5.040 keV
10.2 >
FS= 63
ch 262= 3 cts
MEM1:

Fig 1.6.

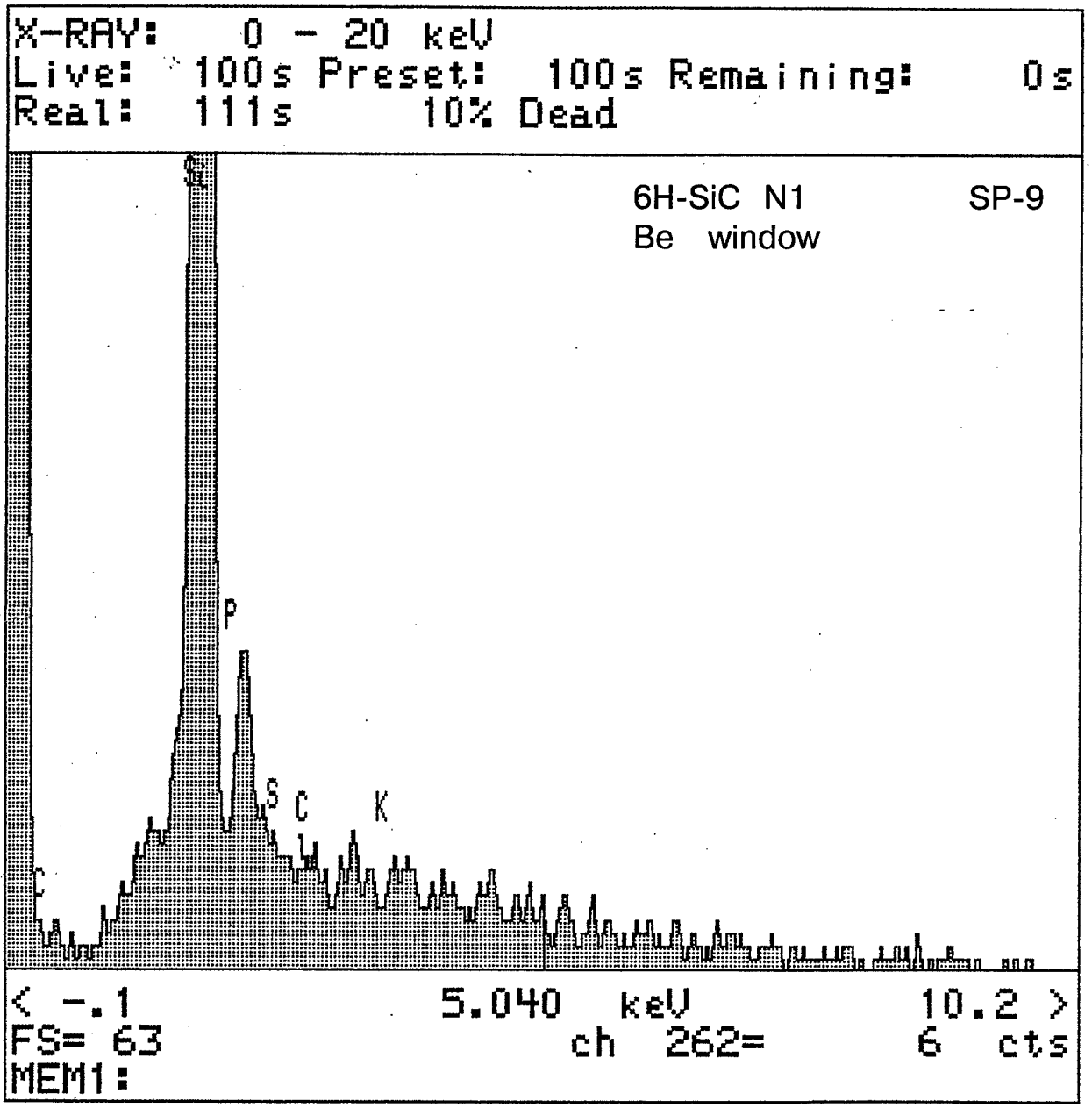
X-RAY: 0 - 20 keV
Live: 100s Preset: 100s Remaining: 0s
Real: 111s 10% Dead
6H-SiC N1 SP-9
Be window
Si
P
S
C
K
C
< -.1 5.040 keV 10.2 >
FS= 63 ch 262= 6 cts
MEM1:

Fig 1.7.

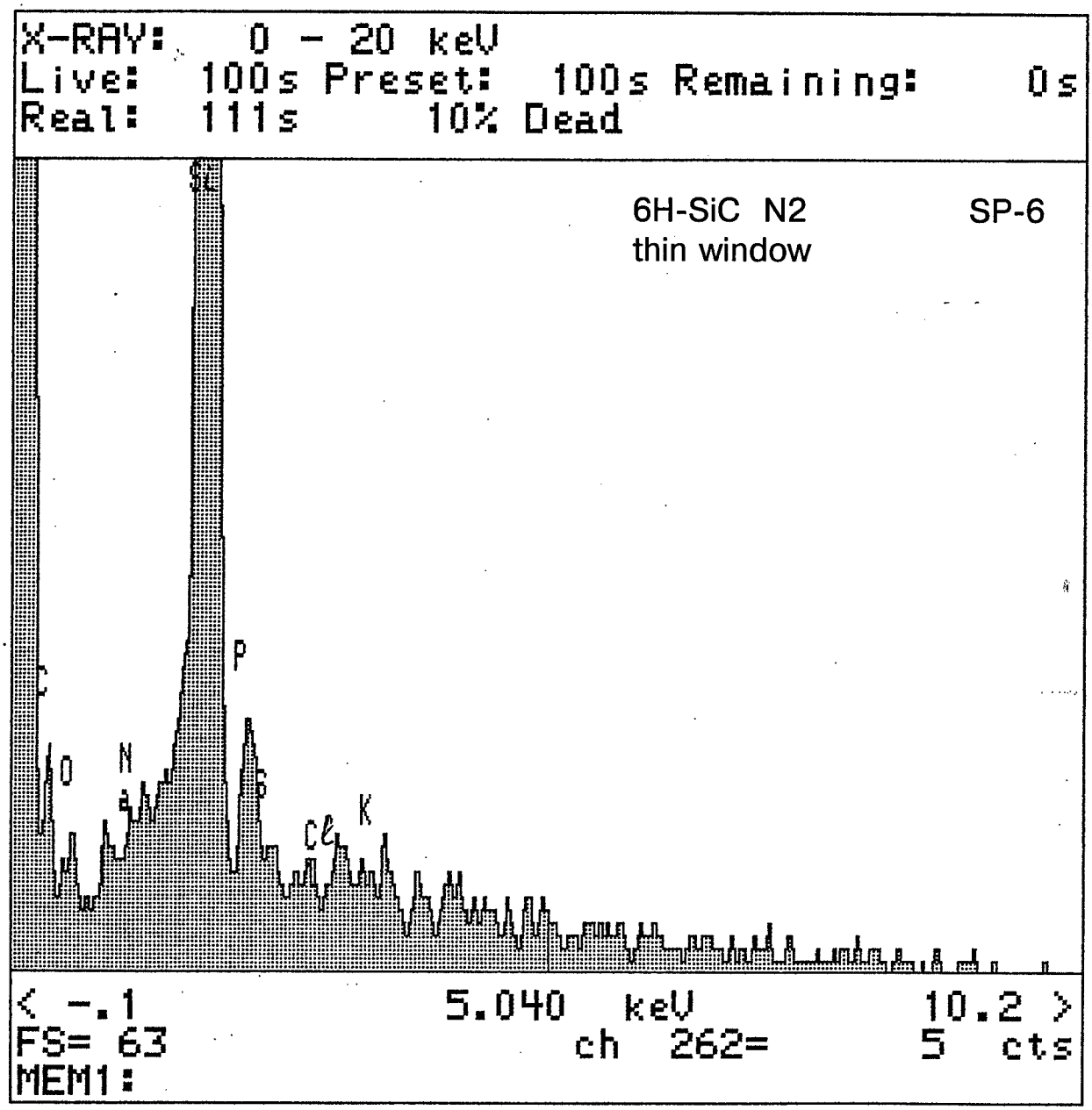
X-RAY: 0 - 20 keV
Live: 100s Preset: 100s Remaining: 0s
Real: 111s 10% Dead
6H-SiC N2
thin window
SP-6
Si
P
O
N
Cl
K
< -.1
5.040 keV
10.2 >
FS= 63
ch 262= 5 cts
MEM1:

Fig 1.8.

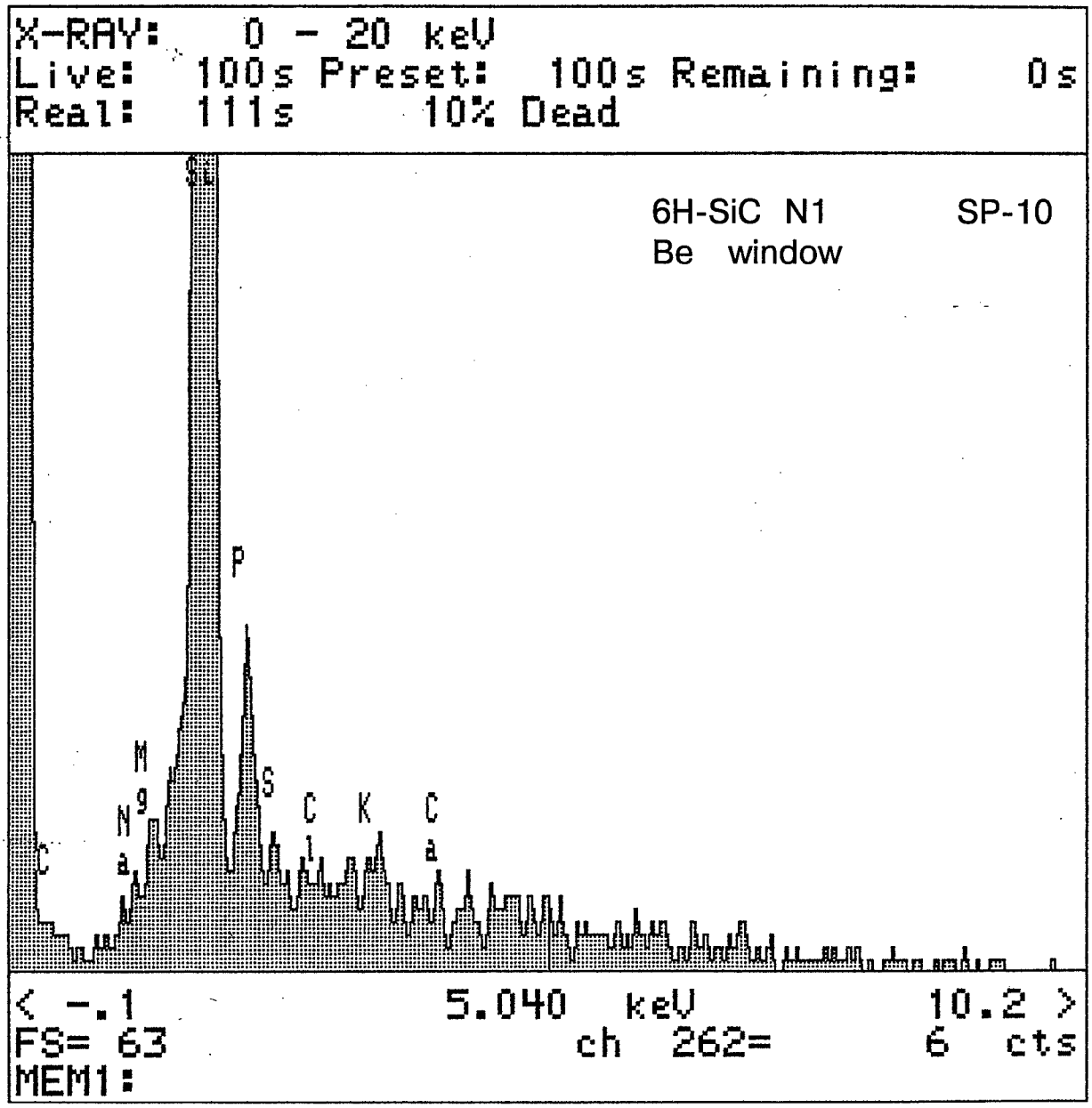
X-RAY: 0 - 20 keV
Live: 100s Preset: 100s Remaining: 0s
Real: 111s 10% Dead
6H-SiC N1 SP-10
Be window
Si
P
S
Mg
Na
Cl
K
Ca
C
< -.1 5.040 keV 10.2 >
FS= 63 ch 262= 6 cts
MEM1:

Fig 1.9 .

Fig.1.10b is a topographic pattern of a sample along its depth. The regions with a light contrast are damaged regions of the crystal. After etching along the depth down to dt=5 μm elastic deformations have decreased and it has become possible to observe a defect structure of the entire volume. It is seen that the sample No.1 (6H-SiC) is a perfect crystal containing in all 8 dislocations which are originated from a polytype inclusion. Moreover, concentrated in the central part of the sample are inclusions of unknown character.

Fig.1.11 presents the topographic patterns for two samples of 6H-SiC. The sample No.2 is characterized with three plane dislocation clusters lying at different depths. The major centers of dislocation generation are concentrated near to a crystal "leg" which is a place where a crystal adheres to the crystallization bush of the growth furnace.

16

It is convenient to measure the dislocation density N_d in plane clusters using its number per length unit instead of a number per area unit as in the case of a random distribution. Expediency of such an approach is evident from Fig.1.11b obtained by the "hold-frame" method for the sample No.2. As seen from this figure, various dislocation clusters lie at different depths in a sample. The dislocation density in such clusters is N_d=10 to 100 cm^{-1}.

The crystal No.3 is the least perfect. Its majority of dislocations have a loop-like form and they are generated by inclusions of another phase.

The samples No.4 and 5 (15R-SiC) are quite perfect and they have small densities of dislocations whose ends come out on the lateral sides (Fig.1.12) .

Thus, the single crystals of 6H and 15R-SiC prepared by the sublimation method are quite perfect. Most of them have small (N_d=10 to 100 cm^{-1}) density of basal dislocations.

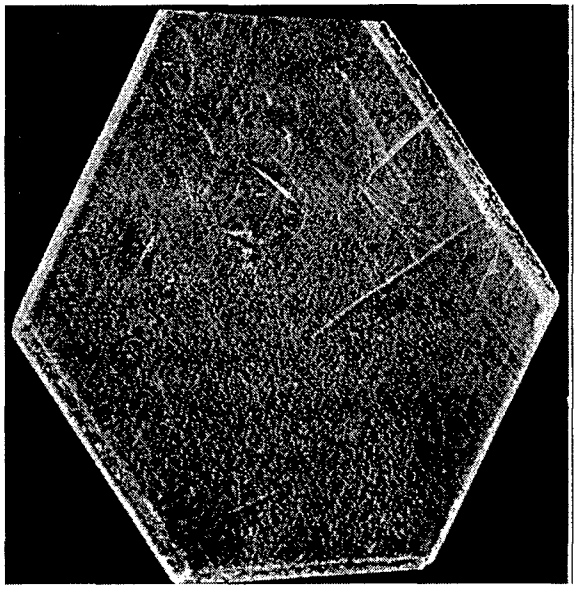

a

c

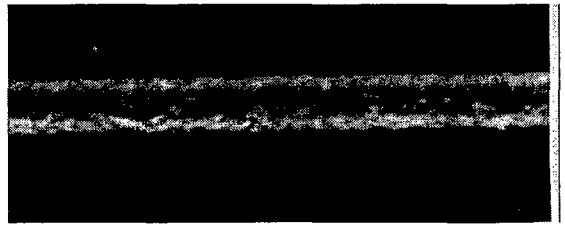

b

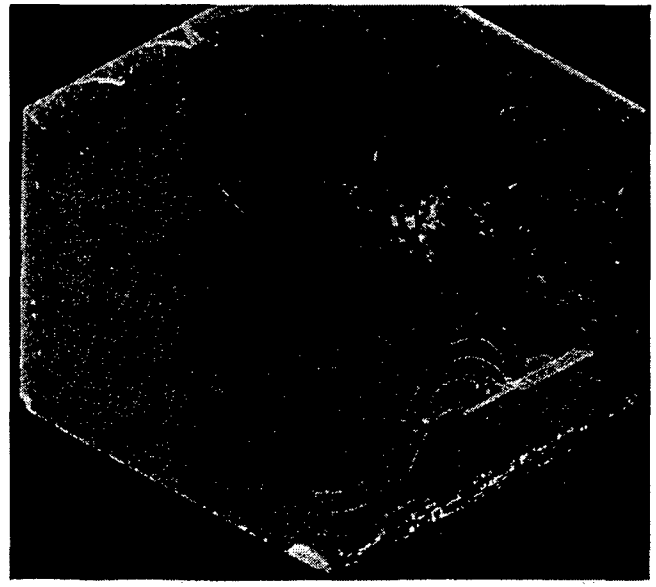

d

Fig.1.10.Projection topographic patterns(a,b) and "hold-frame" transmitting topographic patterns (b,c) for sample № 1 $MoK\alpha_1$, $\{\bar{1}120\}$ - reflex. a,b - after mechanical ground and polishing; c,d - after chemical etching.

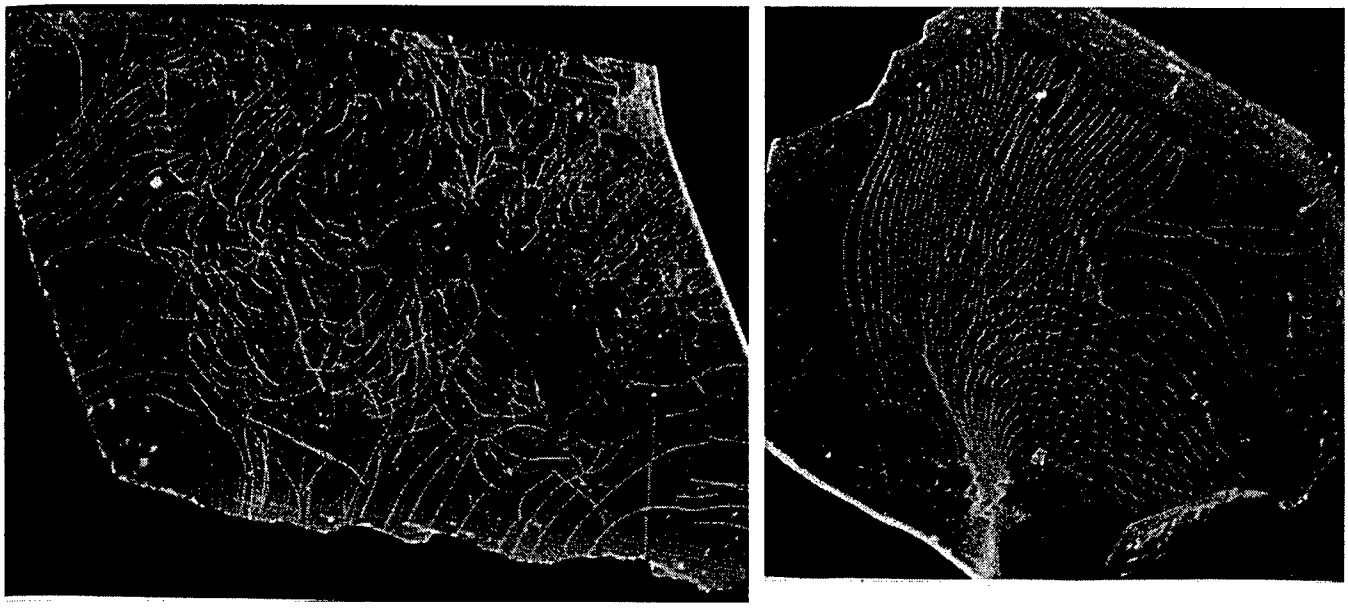

a b

c

Fig. 1.11. Projection (a, c) and "hold-frame" transmit (b) topographic patterns. MoKα_1,$\{\bar{1}120\}$- reflex. a, b - crystal № 2, c - crystal № 3.

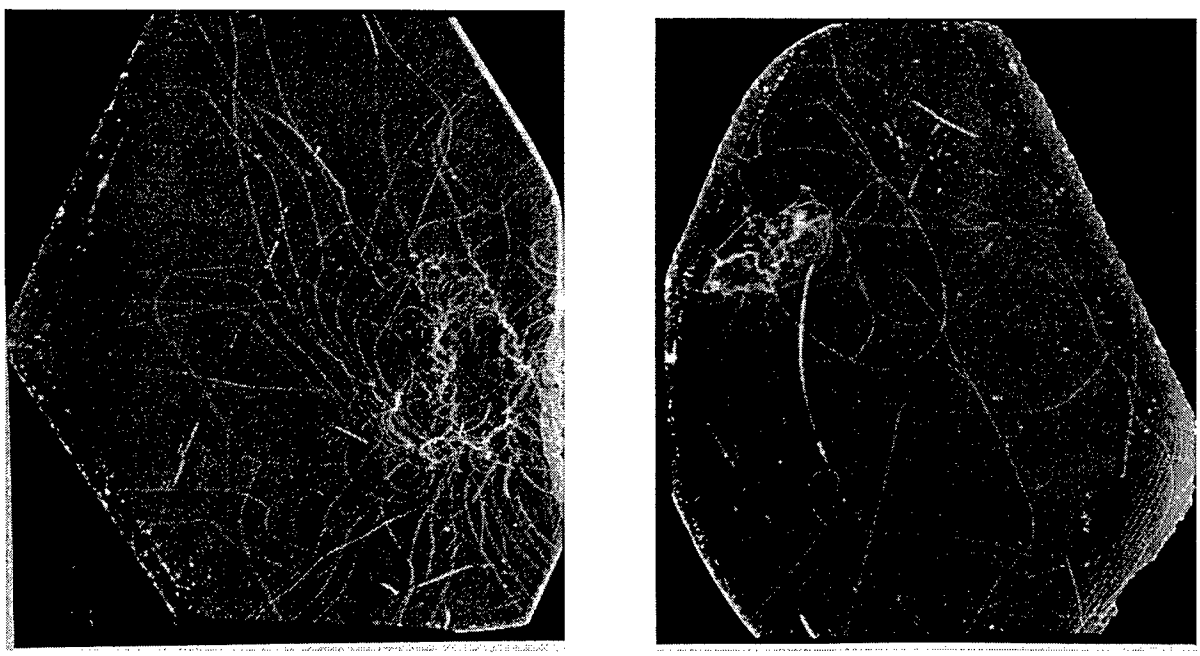

a b

Fig. 1.12. Projection topographic patterns sample № 4 (a) and sample № 5 (b). MoKα_1,$\{1\bar{1}20\}$- reflex.

1.4.3. Identification of SiC-polytypes by the Raman Scattering and X-ray diffractometric methods

The spectral features of optoelectronic devices on SiC depend on the polytype used. The latter one is identified commonly by the spectral position of impurity luminescence bands. But the intensity of the characteristic luminescence at the room temperature is high only at a large enough impurity content. On the other hand, the spectral half width of these luminescence bands is large enough and this fact results in a bad accuracy, especially for specimens that contain several polytypes. Such polytype splices are natural heterostructures and therefore maybe practically important in some optoelectronic devices.

As an alternative method to identify SiC polytypes one can use the method based on the Raman Scattering (RS). If it is implemented using a focused laser beam for excitation then it gains advantage over the luminescence and X-ray diffractometric methods. The latter is related with a high space resolution of Raman Scattering and as a result with a possibility to check small inclusions of another polytype in a sample.

It is known that all the SiC polytypes are characterized by the general phonon dispersion in the standard large Brillouin zone, but the frequencies of phonon lines in the Raman spectra are specific for every polytype [14]. From this point of view a certain polytype may be considered as a natural superlattice with a specific period. The most convenient way to use this fact for diagnostics is measuring the Raman spectra in the frequency region of "folded" acoustic phonons, due to a large dispersion of acoustic phonon branches.

With a view to identify a polytype composition of the SiC splices we have carried out investigations of the Raman spectra for a number of samples. Along with it, we have measured the photoluminescence spectra excited by the nitrogen laser

radiation(λ=337.1 nm). The Raman spectra were recorded with the ДФС-24 spectrometer. An excitation source was the argon laser (λ=488.0;514.5 nm). A laser beam was directed along the c axis with a view to obtain scattering by phonons of all the polytypes which are present in a splice along the given direction.

Presented for illustration (Fig.1.13) is the Raman spectrum for the sample which, according to the photoluminescence data from opposite faces, is assigned to a splice of the 6H and 21R polytypes. It is seen that in this Raman spectrum in addition to appropriate phonon lines 148 cm^{-1} (6H polytype) and 130 cm^{-1} (21R polytype) manifested is also the intensive peak 172 cm^{-1}, corresponding to the 15R polytype (with a view to compare, Fig.1.13 presents also the Raman spectra for pure polytypes). Thus, the RS method has enabled to obtain more complete information on the splice polytype composition. One may conclude that the 15R polytype layer is situated inside the sample and the surface layers at both splice sides are formed by the 6H and 21R polytypes. Moreover, since the RS cross-sections for the characteristic phonons under consideration are nearly equal for different polytypes, then the RS line intensity relationship gives an information on the ratio of polytype thicknesses in the splice. The prevailing bulk part of the sample under consideration consists of the "internal" 15R polytype which has not been found in the spectra of photoluminescence from its faces.

Similar investigations of RS have been carried out for a number of splices containing several combinations of the following polytypes: 4H, 6H, 8H, 15R, 21R. In the cases when the samples consist of two polytypes, we observed a correlation with the photo luminescence data. For the splices consisting of three and more polytypes, with a view to check the Raman spectra we have analyzed a polytype composition using the diffractometric method proposed in [15].

Since the samples under study are plates parallel to the (0001) plane, then the analysis of a polytype structure

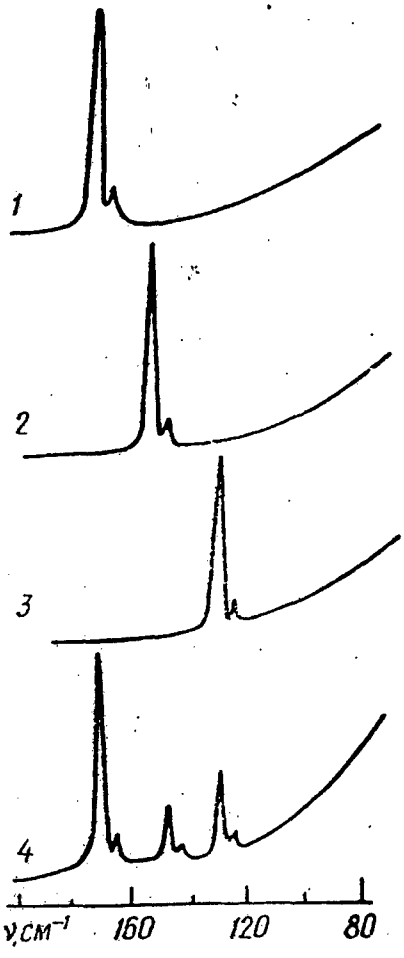

Fig.1.13. RS Spectrum fragment for the pure SiC polytypes: 15R(1), 6H(2), 21R(3) and polytype splice 15R+6H+21R(4)

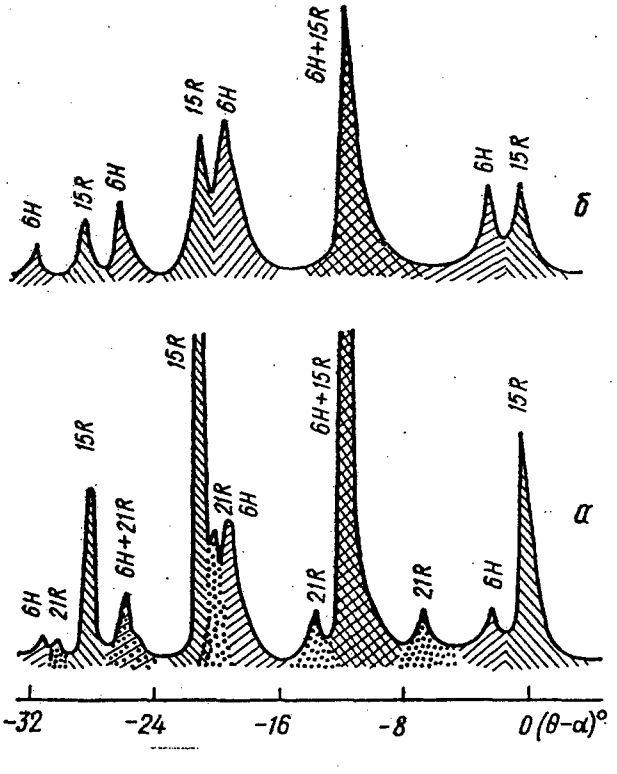

Fig.1.14. Diffraction patterns for the SiC polytype splices: 15R+6H+21R(a), 6H+15R(b)

is carried out as following from the angle difference $\omega=\theta-\alpha$ (θ is the angle between a crystal plane and the c axis, α is the Bragg angle). The diffractometric analysis was carried out using the X-ray goniometer and MoK_α-emission.Since for the sample understudy one observes the Laue diffraction of X-ray emission, we studied the entire volume.

In the diffraction pattern shown in Fig.1.14a we can see the reflexes (01.2), (01.5), (01.8), (01.11) of the 15R polytype;(10.1), (10.2), (10.3), (10.4), (10.5) of the 6H polytype and(01.5), (01.8), (01.11), (01.14), (01.17) of the 21R polytype.In accordance with RS data the diffraction pattern presented gives evidence that the prevailing part of the sample consists of the 15R polytype and the 6H and 21R polytypes are present with a considerably less amount. Shown in Fig.1.14b is the diffraction pattern for the sample with approximately identical percentage of the 6H and 15R polytypes. The diffractometric analysis data for all the samples studied have entirely confirmed the results of a polytype composition identification for the SiC splices made by the RS method.

Especially convincing advantages of the RS-method manifest themselves with using the MicroRaman analysis. Focusing the exciting laser beam in a 1 μm size spot enables to check polytype interfaces in a splice with a high space resolution.

In such experiments we have used the triple additive monochromator Dilor (OMARS 89, XY), precision ~ 1 μm, with the Olympus microscope (x10, x50, x100 objectives) and CCD camera as a multichannel detector (1024 pixels 25x2500 μm^2 intensified by the microchannel tube), the S25 entrance photocathode.

Fig.1.15 presents some RS spectra from a cross-section of the splice which contains three polytype layers (15R+6H+15R). The cross-section of the splice studied is shown schematically in Fig.1.16.

The spectra No.1, No.10 and No.19 in Fig.1.15 correspond to

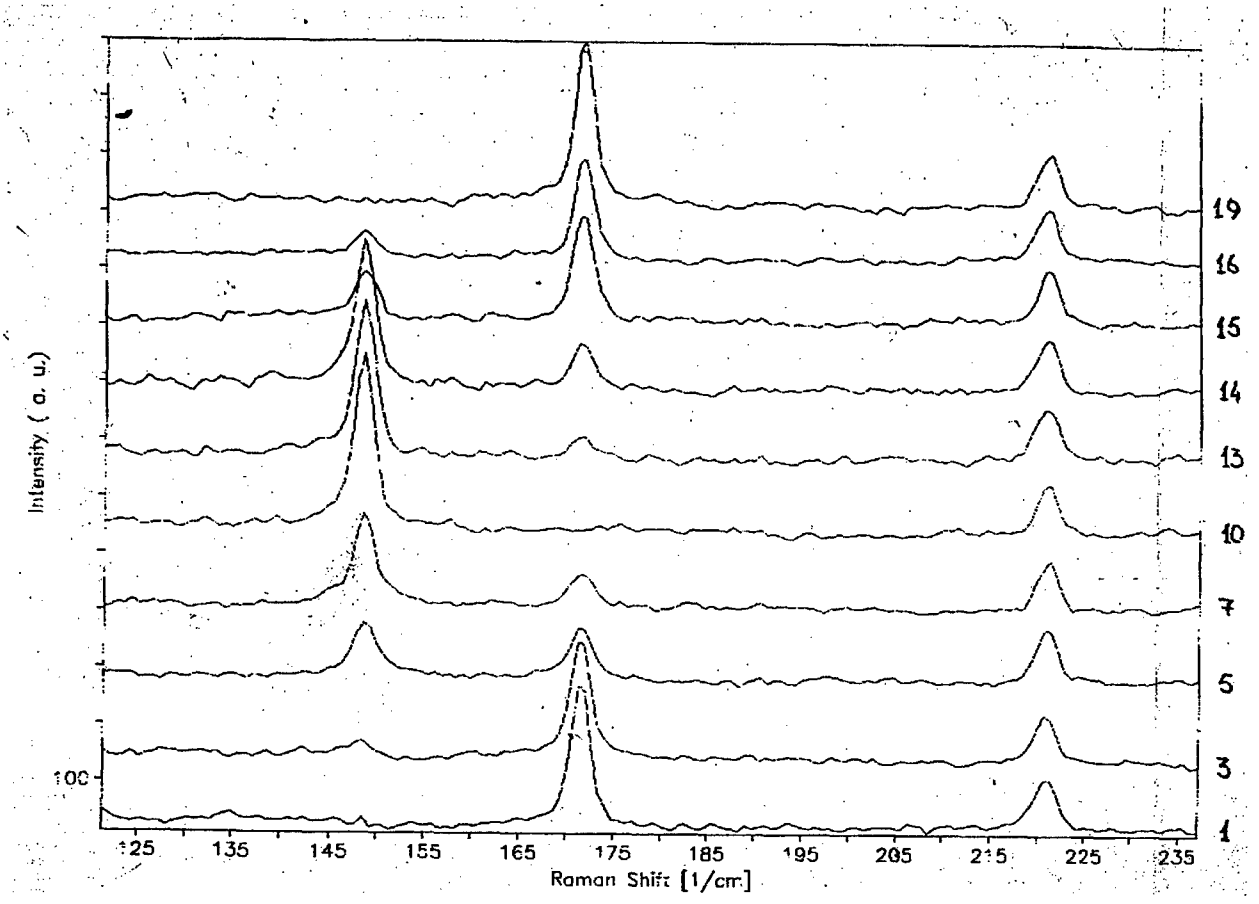

Fig.1.15. RS spectra from a cross-section of the splice which contains three polytype layers (15R+6H+15R)

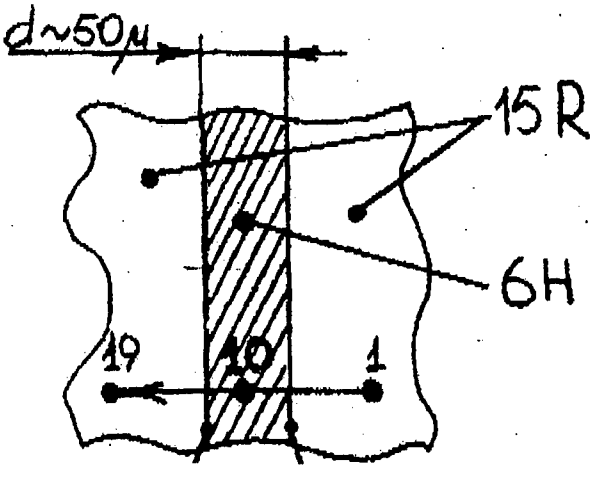

Fig.1.16. The cross-section of the splice which spectra are shown on Fig.1.15.

the points No.1, No.10 and No.19 in the first (15R), second (6H)and third (15R) layers of the sample at a distance from polytype interfaces. The rest spectra are obtained with the 0.25 μm step near to the first (No.3, No.5, No.7) and the second (No.13,No.14, No.15, No.16) polytype interfaces. The line 221.04 cm^{-1} in all the spectra is the Ar^{+} plasma line which was used as a reference point.

1.4.4. Spectrum of nitrogen in 6H and 15R SiC.

ESR spectra of nitrogen are studied for 6H and 15R SiC samples produced by means of Lely method, contained nitrogen in concentrations of 10^{16}– 10^{19} cm^{-3}. Measurements were carried out by the EPR spectrometer with operation frequency 140 GHz. The high microwave field frequency and the presence of a static magnetic field up to 7.4 T, generated by a superconducting magnetic system with a high homogeneity (10^{-5} per 1 cm^{-3}), made it possible to investigate ESR spectra with an extremely high resolution in terms of the g-factor.

The relative values of the g-factor of the unknown spectra were determined to within $2 * 10^{-5}$ (when the width of an absorption line was 5 G). The adopted procedures made it possible to ensure a high sensitivity of the spectrometer when single crystals of 10^{-4} cm^3 volume ($5*10^8$ spins/G) were used [16].

The ESR spectrum of 6H and 15R SiC samples with nitrogen concentration from $2*10^{16}$ to $7*10^{16}$ cm^{-3} and different degrees of compensation consisted of two for 6H and three for 15R triplets of the hyperfine structure lines (Ik1, Ik2, Ik3) due to the nitrogen nuclei ^{14}N, corresponding to two for 6H SiC and to three for 15R SiC in equivalent cubic position of nitrogen, as well as a single line Ih1 for 6H SiC and Ih1, Ih2 for 15R SiC with an anisotropic width corresponding to the hexagonal position of nitrogen (Fig.1.17a, 1.18a) [16].

The appearance of the Ih1 for 6H SiC and Ih1, Ih2 for 15R SiC

ESR spectrum of nitrogen in 6H SiC

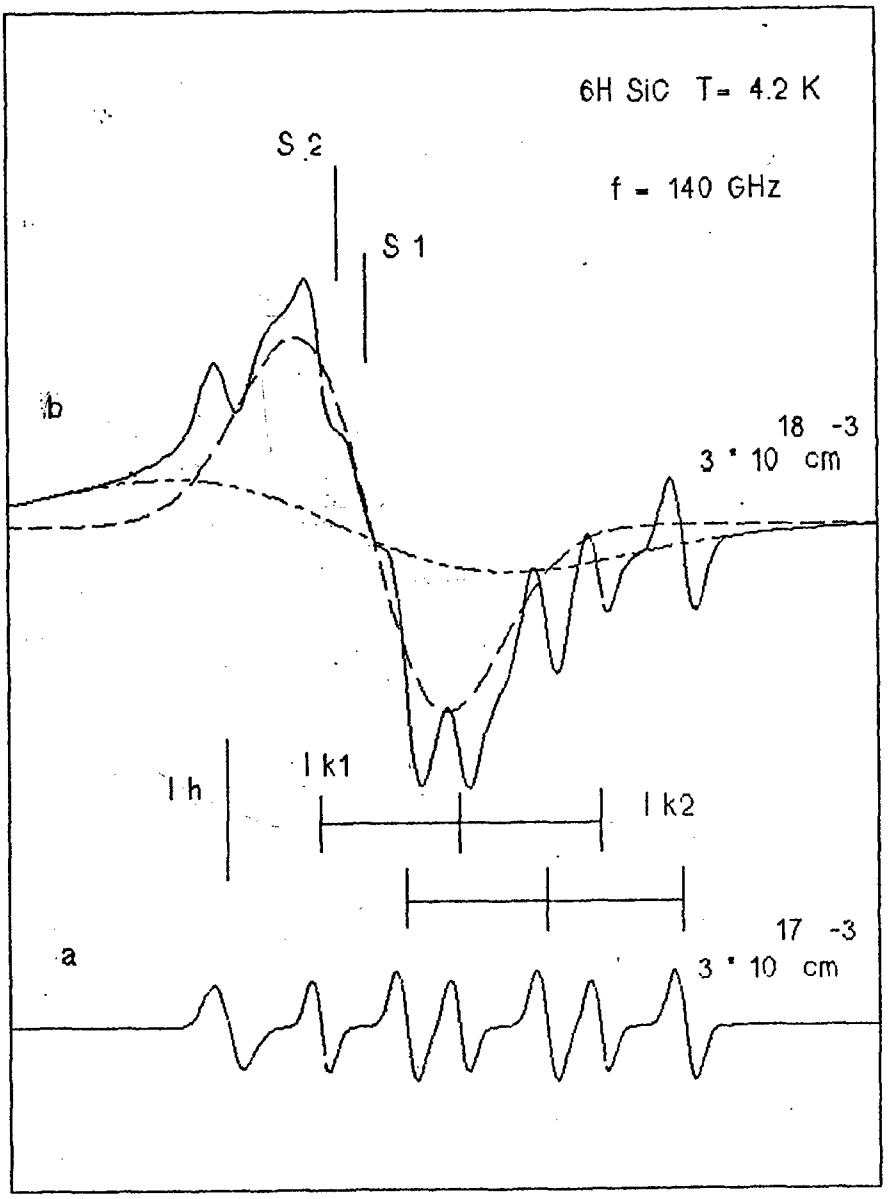

Fig. 1.17

ESR spectrum of nitrogen in 15R SiC

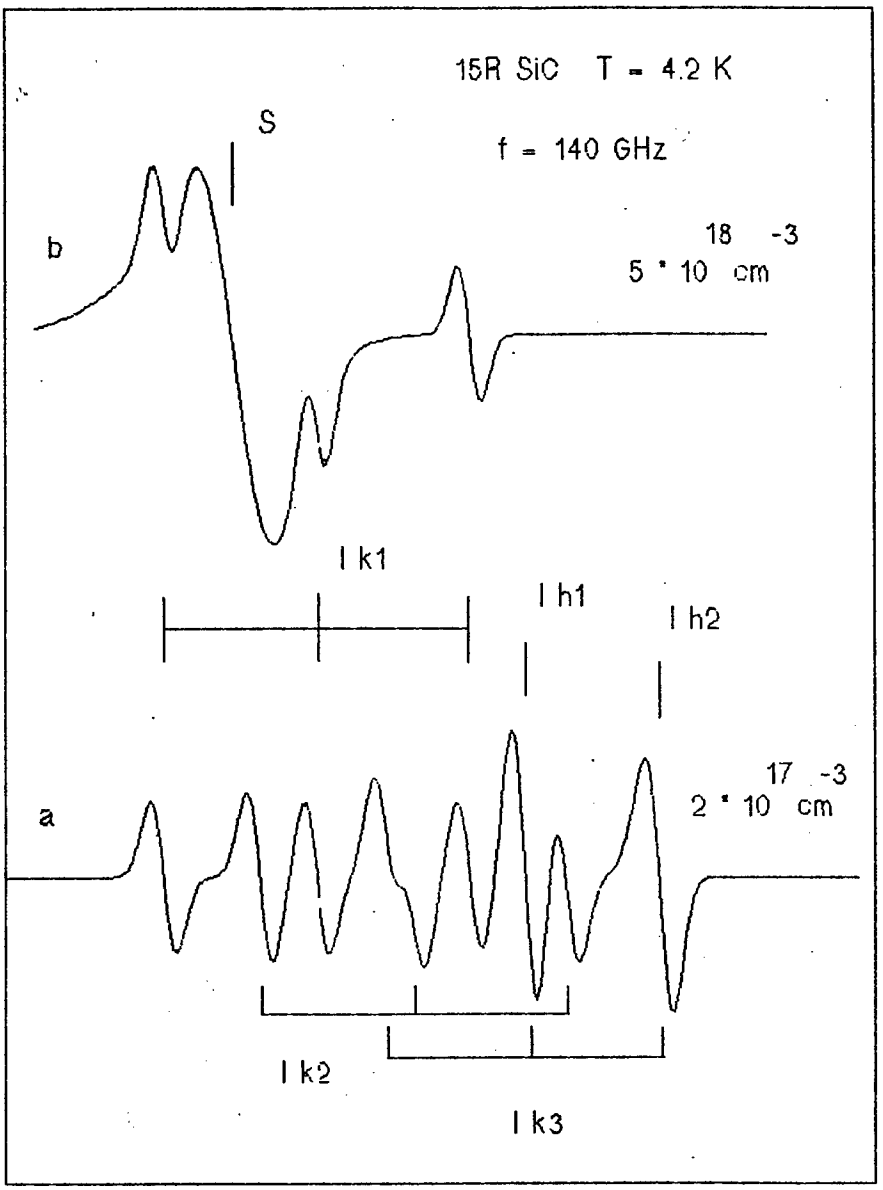

Fig. 1.18

line in the ESR spectrum and the intensity of this line depended on the degree of compensation of the investigated samples [17].

An increase in the nitrogen concentration N_N modified the observed spectrum. It clear from Fig.1.17b,1.18b that when N_N was increased up to $5*10^{17}$ cm^{-3}, an additional wide S-line appeared against the background of the spectrum of single centers in 6H and 15R crystals. The S-line position did not correspond to the center of gravity of the ESR spectra of the cubic and hexegonal nitrogen positions nor to the center of gravity of these spectra. The S-line has an asymmetric profile and an anisotropic g-tensor. Its intensity was much higher then the sum of the intensities of the absorption lines of isolated nitrogen atom.

The further growth of the concentration of nitrogen up to 10^{19} cm^{-3} results in the shift of all nitrogen ESR lines in 6H and 15R SiC towards the S-line and, at last, one observes the only S- line in ESR spectrum.

Analyse of exchange line in 6H-SiC show that S-line consist of two S1 and S2-lines with different width and intensity (Fig.1.17b). At T = 4.2 K g-value of S1-line corresponds to the average value of the Ih1 and Ik1 ESR spectra whereas the g-factor of S2-line corresponds to the average value of the g-factor of the Ih1 and Ik2 ESR spectra. As shown from the temperature dependence of the g-value of S1 and S2-lines (Fig.19), g-value of S1 and S2-lines approaches the g-value of EPR spectra of cubic position Ik1 and Ik1 correspondly at 77 K. Fig.1.20 shows the temperature dependence of the intensity of the S1 and S2 line in the temperature interval 4.2 - 40 K. The intensity increases with lowering temperature according to the Curie low:

$$I(T) \sim C/T \qquad (1.1)$$

This data are consistent with the date obtained for 6H SiC in [18].

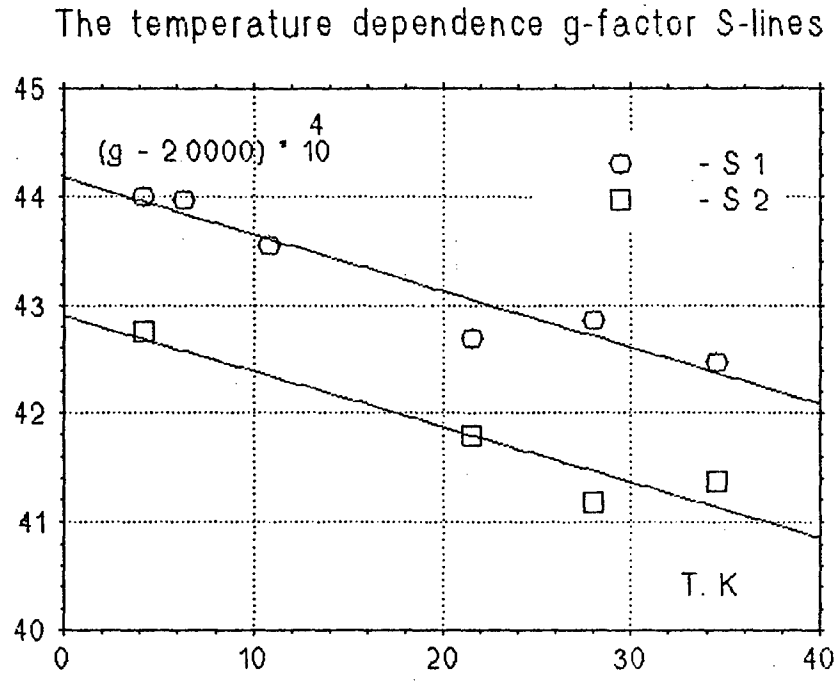
The temperature dependence g-factor S-lines
45
44
43
42
41
40
0
10
20
30
40
4
(g - 2.0000) * 10
- S 1
- S 2
T. K

Fig. 1.19

The temperature dependence of the intensity of the S-line

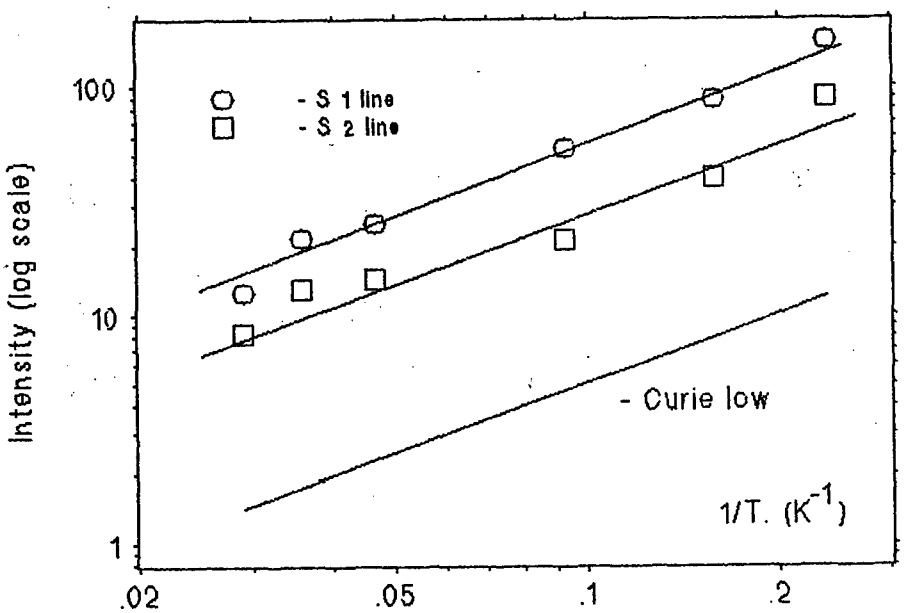

Fig. 1.20

The S1 and S2-line width depends on temperature. Fig.1.21 shows the temperature dependence of the S1, S2-line width in the temperature interval 4.2 - 40 K. When temperature increase from 4.2 to 35 K the S1 and S2-line width decreases. A similar behavior of temperature dependence of the exchange line width was observed for Si heavily doped with phospour, described by expression [19]:

$$dH \sim \exp(2R_0 / a_0) * \tanh(D/kT) \quad (1.2)$$

Where R_0 , a_0 and D are the inter donor distance; effective Bohr radius and the potential difference between an occupied site and an unoccupied site, respectively.

For 6H SiC a_0= 5 - 7 Å [20]. The temperature dependence for S1 and S2-line are in accordance with equation (1.2) with parameters of R_0= 14 Å, D= 50 K for S1- line and R_0= 12 Å, D = 52 K for S2- line.

These data suggests that the electrons spend most of the time at the donor sites. The probability of the direct Heizenberg exchange between the paramagnetic nitrogen centers was very low, but the probability that paramagnetic nitrogen atom encountered a nonparamagnetic nitrogen atom in the same of the nearest unit cell of the crystal was high. This elementary jump was on the one hand, an essential part of the hopping conduction process and, on the other hand, it ensured hopping exchange of a donor electron between two paramagnetic systems. As shown in [17] at high donor concentrations and high degree of compensation were many ionized nitrogen centers at the hexagonal positions, which were nonparamagnetic. Therefore the probability that paramagnetic nitrogen atom at the cubic position encountered a nonparamagnetic nitrogen atom in the hexagonal position was high.In this case donor electron could be captured from a cubic by a hexagonal nonparamagnetic nitrogen atom that the latter became paramagnetic. Consequently, the position of the exchange line in the ESR spectrum of nitrogen in

The temperature dependence of the line width.

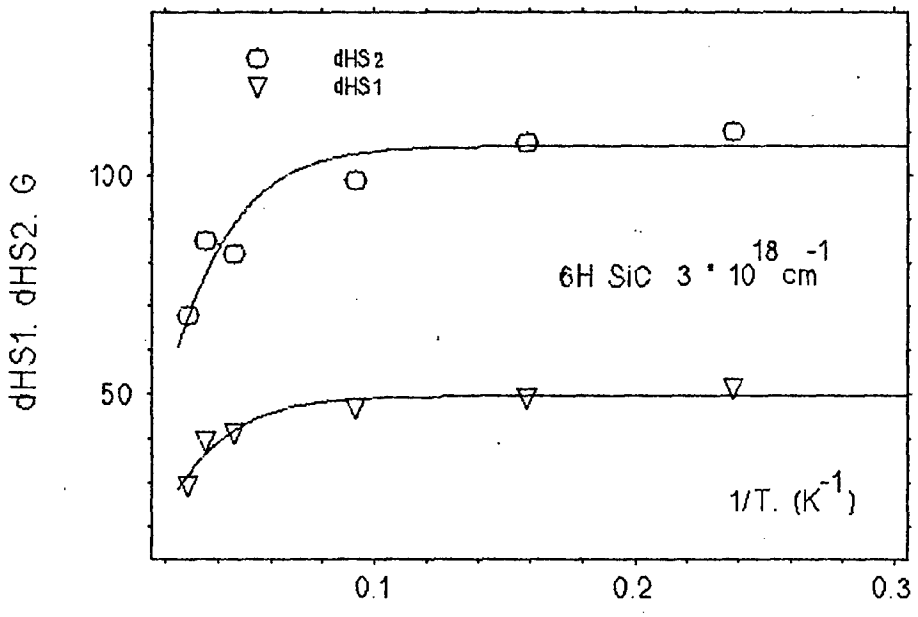

Fig. 1. 21

the hexagonal polytype of SiC was governed by the nitrogen concentration by the degree of compensation of the sample, by the ratio of the depths of the energy levels of the hexagonal and cubic center in the band gap and by the value of the effective Bohr radius of the donor elect- ron.

It is clearly follows from the temperature dependence of the g-value of S1 and S2-exchange lines. As the temperature increase the ionized nitrogen centers at the cubic position were appeared, probability of the exchange hopping motion between paramagnetic and nonparamagnetic atom in one cubic position was increased and g- value of S1 and S2-line shifts to the center gravity of the ESR spectrum of nitrogen at the cubic position.

This feature suggests that the mechanism of hopping motion for donor electron in 6H SiC heavily doped with nitrogen is working.

The nature of the low-temperature conductivity of 6H SiC was investigated earlier in [18] and it was established that between 4.2 K and 25 K the low governing the electrical resistivity of the sample with the nitrogen concentration 10^{19} cm^{-1} was typical of variable-range hopping too.

1.4.5.Surface electron properties of the 6H and 15R modification silicon carbide

The investigation was carried out with the n-type samples of single-crystal silicon carbide, 6H- and 15R-modifications,with the nitrogen impurity concentration of $9*10^{17}$ and $3*10^{18}$ cm^{-3},respectively [20-22].Their large faces (0001)Si and (0001)C were ground and then polished using diamond pastes. In order to remove a layer with mechanical structural damages, the samples underwent oxidation at 700°C in a humid oxygen flux for a few tens of minutes. Then the oxide layer was etched in the CP-4 etcher ($HF:HNO_3:CH_3COOH \cong 3:5:3$). Afterwards, the samples were electrolytically oxidized in the 5 % solution of KNO_3 in ethyleneglycol for 10min. The samples electrolytically oxidized underwent studies of the surface potential vs temperature

dependencies. The study was repeated after removal of the oxide layer obtained electrolytically by processing in HF. Then after etching the samples in KOH at 650 ^{o}C we carried out identification of the $(0\bar{0}01)$Si and (0001)C surfaces according to their characteristic appearance [23] using an optical microscope.

The surface potential ϕ_s (energetic band bending at surface) was determined by the method of measuring the surface photovoltage under the conditions of a large level of electron-hole pair generation by light pulses of the ИСШ-100 flash lamp (illumination intensity ~10^{21} quanta/cm^2 s) which straightens bands at a semiconductor surface at the moment of illumination [24]. For this purpose we mounted in a cryostat the measuring capacitor consisting of a mica plate with the SnO_2 semitransparent layer deposited on mica. A sample of SiC was attached with one of its surfaces to another side of the micaplate. The photovoltage signal was recorded by a storage oscilloscope that enabled, taking into account the calibration coefficient of the circuit, to determine the ϕ_s value.

The temperature dependence $\phi_s(T)$ was recorded under the vacuum 10^{-4} Pa with lowering temperature from 300 to 100 K. In the most cases already at the room temperature we have found the surface potential photomemory effect [25]. It consists in the fact that after illumination of a sample by the first lightpulse one observes a capture of minority carriers (holes) at the surface traps which results in variation of ϕ_s after action of a light pulse. As a result, using the second or any other subsequent light pulse one measures already a changed value of ϕ_{s2} which is less by absolute magnitude as compared with the ϕ_{s1} value measured using the first light pulse. The difference $|\phi_{s1} - \phi_{s2}|$ determines the surface potential photomemory. Under the conditions of our experiment it was determined at the light pulse repetition frequency equal to 1 Hz.

It should be noticed that the ϕ_{s2} value determined using the second pulse was equal to that for the third or any other subsequent pulse. This gives evidence that traps capturing

nonequilibrium holes are saturated with them already under illumination by the first light pulse. The ϕ_{s1} value corresponding to the dark conditions can be determined at a certain temperature only after emptying traps with captured holes which demands to wait a certain time after a previous illumination or to reheat a sample. Below the room temperature the period of storage of the holes captured in traps considerably increases (hours). Therefore, for correct determination of the ϕ_{s1} and ϕ_{s2} dependencies on temperature every time after measuring at a certain temperature we carried out reheating a sample up to temperatures above 300 K with subsequent cooling in dark down to a temperature for new measurements of ϕ_{s1} and ϕ_{s2}.

1. Fig.1.22 and 1.23 present the temperature dependencies of the surface potential: ϕ_{s1} (curves 1, 2) and ϕ_{s2} (curves 1', 2'), respectively for the SiC-6H and SiC-15R surfaces. The dependencies for the $(000\bar{1})$Si surfaces are given in Fig.1.22a and1.23a. Those for $(000\bar{1})$C are given in Fig.1.22b and 1.23b. The curves 1,1' are obtained for the surfaces etched electrolytically, the curves 2, 2' - for the surfaces processed after that in HF. The ϕ_{s1} and ϕ_{s2} values are always negative. As following from calculations, this means that with all kinds of processing then-SiC-6H and 15R surfaces a surface layer depleted with electrons is formed at these surfaces. The depletion decreases after illumination of a sample by the first light pulse since the ϕ_{s2} value by absolute magnitude are always less than corresponding values of ϕ_{s1}.

The behavior of the surface potential vs temperature dependencies $\phi_{s1}(T)$ is different. For the (0001)Si surfaces of SiC-6H and 15R they have an N-like form. For the $(000\bar{1})$C surfaces they are V-like. At the same time, the N- and V-like forms for various polytypes and surfaces are different. The increase of $|\phi_{s1}|$ with lowering temperature, which is always observed near to the room temperature, is related to filling-in the fast surface electron states (SES) with electrons in consequence of shifting the Fermi level in a semiconductor to the c band. The decrease of

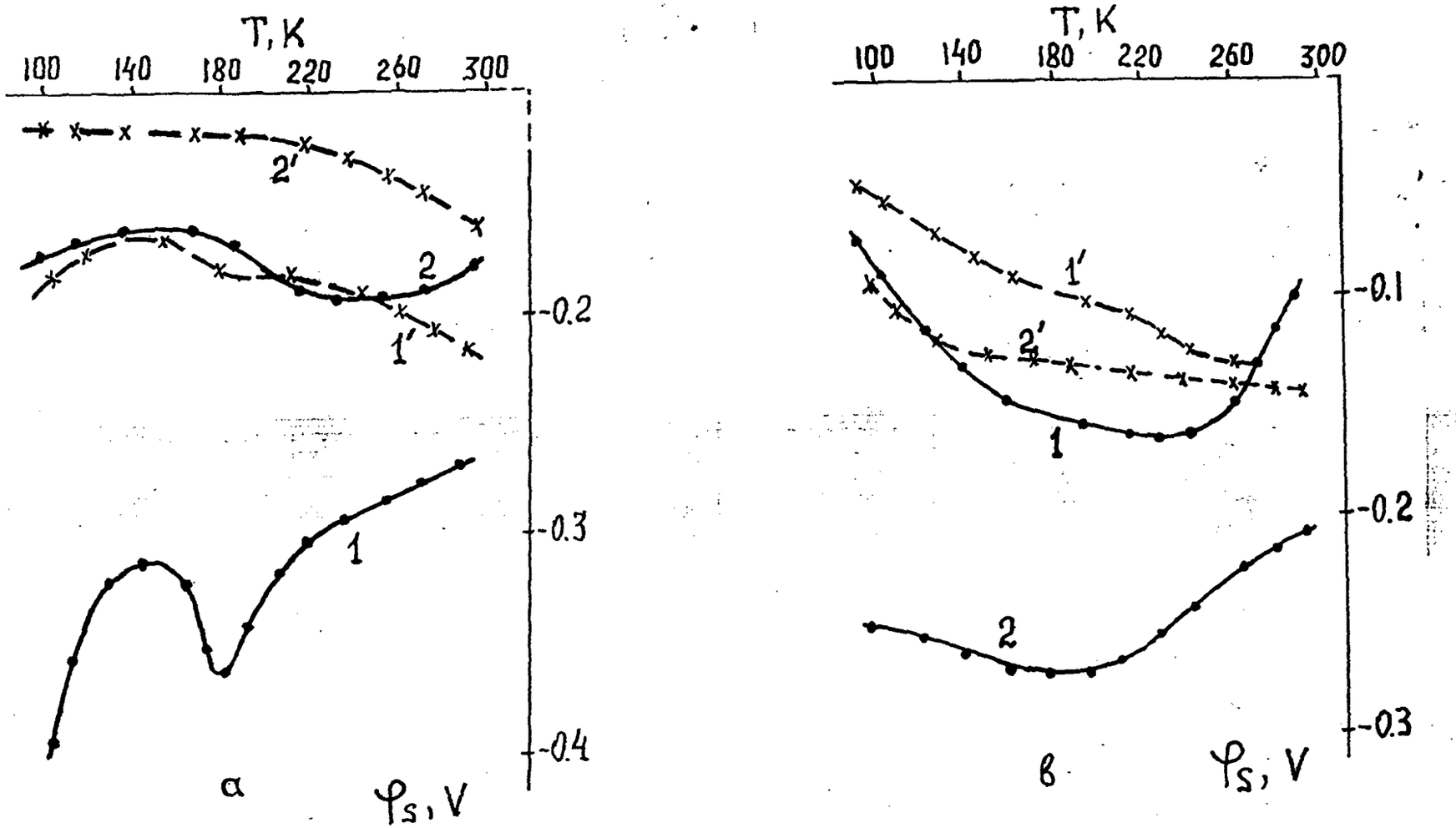

Fig.1.22.Temperature dependencies of the surface potential ϕ_s on the (0001) Si (a) and ($\bar{0}\bar{0}01$) C (b) surfaces of SiC-6H : Surface processing : 1,1' - oxidized electrolytically; 2,2'- processed in HF . 1,2 - ϕ_{s1} ; 1',2' - ϕ_{s2} .

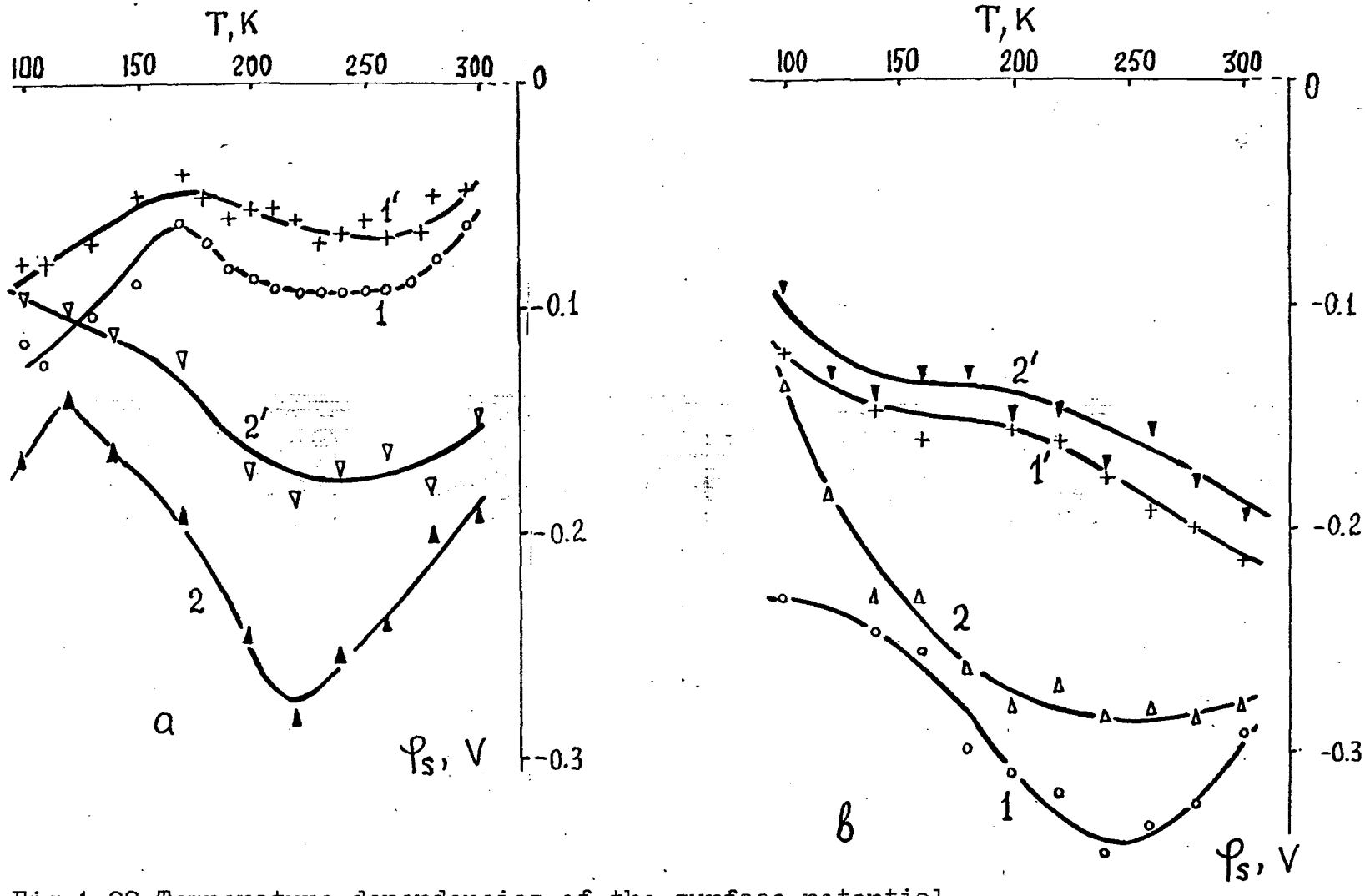

Fig.1.23.Temperature dependencies of the surface potential ϕ_s on the (0001) Si (a) and ($0\bar{0}01$) C (b) surfaces of SiC-15R. Surface processing : 1,1' - oxidized electrolytically; 2,2'- processed in HF . 1,2 - Φ_{s1} ; 1',2' - Φ_{s2} .

$|\phi_{s1}|$ observed at lower temperatures is related to decreasing the negative charge in SES. It may be explained only assuming that with lowering temperature the fast SES system is reconstructed itself. We observed a similar phenomenon earlier at certain physical and chemical conditions of the germanium [26,27], silicon [28,29] and gallium arsenide [30] surfaces. It was related to reversible structural changes occurring with lowering temperature at a semiconductor interface with a covering oxide film.Reversibility and reproducibility of the $\phi_{s1}(T)$ dependencies were confirmed also by checking measurements for all the surfaces of SiC-6H and 15R.

A different behavior (N-like or V-like) of the $\phi_{s1}(T)$dependencies at the (0001)Si and $(000\bar{1})$C surfaces of SiC-6H and15R is related to features of oxide coverage on them. It is known that the (0001)Si and $(00\bar{0}1)$C planes formed respectively only by the Si and C atoms are covered by the SiO_2 oxide films which are formed under natural air conditions or during special oxidizing processing [23]. For the $(00\bar{0}1)$C surface an oxide coverage is usually uniform, while for the (0001)Si surface it is non-uniform and changing by thickness [23,31]. It should be reasonable to expect that structural changes at the $SiC-SiO_2$ interface would be different with lowering temperature for different characters of oxide coverage. From our point of view,an N-like behavior of the $\phi_{s1}(T)$ dependencies on the (0001)Si surfaces is caused first of all by the SiO_2 oxide coverage non-uniformity. We observed earlier a similar effect on the silicon surface when the oxide coverage uniformity was damaged specially by deposition of gold with a micro island structure.[28]. Processing in HF etches electrolytically the SiO_2 layer formed on the SiC surface, but instead of it under the air conditions thin layers (~10 Å) of a natural SiO_2 oxide are formed which because of their non-uniformity on the (0001)Si surface provide for it an N-like behavior of $\phi_{s1}(T)$ as well,although strongly changed. A different character is also observed for V-like characteristics of the $(00\bar{0}1)$C surfaces,oxidized electrolytically and natural (after processing

in HF),which are covered by more uniform oxide films of SiO_2, having however different thickness before and after processing in HF.

As for absolute values of the surface potential ϕ_{s1} on the(0001)Si and $(0\bar{0}01)$C surfaces of SiC-6H and 15R oxidized and processed in HF, then the situation at first is unexpected.One would think that etching an oxide should lead for all the surfaces to increasing $|\phi_{s1}|$, as it is observed for silicon [28],due to removal of a positive charge built in an oxide. However,such a situation is implemented only on the $(00\bar{0}1)$C surface of SiC-6H (Fig.1.22b) and on the (0001)Si surface of SiC-15R (Fig.1.23a).On the contrary, the values of $|\phi_{s1}|$. on the surfaces (0001)Si of SiC-6H (Fig.1.22a) and $(00\bar{0}1)$C of SiC-15R (Fig.1.23b) decrease after processing in HF. It seems that values of a positive charge built in an oxide are different for the (0001)Si and $(00\bar{0}1)$C surfaces of various SiC polytypes. Moreover, processing in HF leads to formation of different SES systems with predominance of their acceptor or donor character.

38

2. In order to calculate charge variation in SES with lowering temperature, a magnitude of a hole charge captured by surface traps as well as to determine the Fermi level position on surfaces at various temperatures, one should know the temperature dependence of the electron bulk concentration in the semiconductors under study. Investigations of the Hall effect have shown that with lowering temperature in the region 300 to100 K the electron concentration in the conduction band of SiC-6H and SiC-15R changes, respectively, within the limits $(4.2\text{to } 0.2)*10^{17}$ cm^{-3} and $(1.7 \text{ to } 0.2)*10^{18}$ cm^{-3}.

Equal to the charge in SES of a semiconductor, which determine a value of the surface potential ϕ_s, is a charge $Q_{sv}$with an opposite sign situated in a semiconductor region adjacent to surface. A variation of Q_{sv} with temperature (with an appropriate variation of ϕ_s with temperature) has to be equal to variation with temperature of Q_s in the fast SES of a semiconductor. In our case to compute values of Q_{sv} one has to use the theory taking

into account a variation of electron charge in the conduction band and donor states with changing ϕ_{s1} [32]. In this case, Q_{sv} at the surface potentials depleting the region adjacent to surface with electrons is equal to

$$Q_{sv}=q\left(\frac{\varepsilon_k T}{2\pi q^2}\right)^{1/2}\left\{n\left(\exp\frac{q\phi_s}{kT}-1\right)+N_d * \ln\left[\frac{1+\exp\left(\frac{E_d-E_F-q\phi_s}{kT}\right)}{1+\exp\left(\frac{E_d-E_F}{kT}\right)}\right]\right\}^{1/2} \quad (1.3)$$

Here, q is the electron charge, ε is the dielectric permittivity of SiC, n is the bulk electron concentration in the c band of SiC at the temperature T, N_d is the nitrogen donor center concentration, E_d and E_F are the energetic positions of donor centers and the Fermi level, respectively, in the bulk SiC at the temperature T in regard to the middle of the energy gap E_i.

In order to compute Q_{sv} using Eq.(1.3), except of measurement of the ϕ_{s1} value, one has to know for a certain T values of n and E_d-E_F. A value of n was determined from the Hall effect and that of E_d-E_F was determined from the neutrality condition:

$$n=\frac{N_d}{\exp\left(-\frac{E_d-E_F}{kT}\right)+1} \quad (1.4)$$

The calculated values of $Q_q/q=-Q_{sv}/q$ for the (0001)Si and $(\bar{0}\bar{0}01)$C surfaces of SiC-6H oxidized and processed in HF are presented in Fig.1.24 and those for SiC-15R are shown in Fig.1.25.Note again that the dependencies $Q_s(T)/q$ give variation

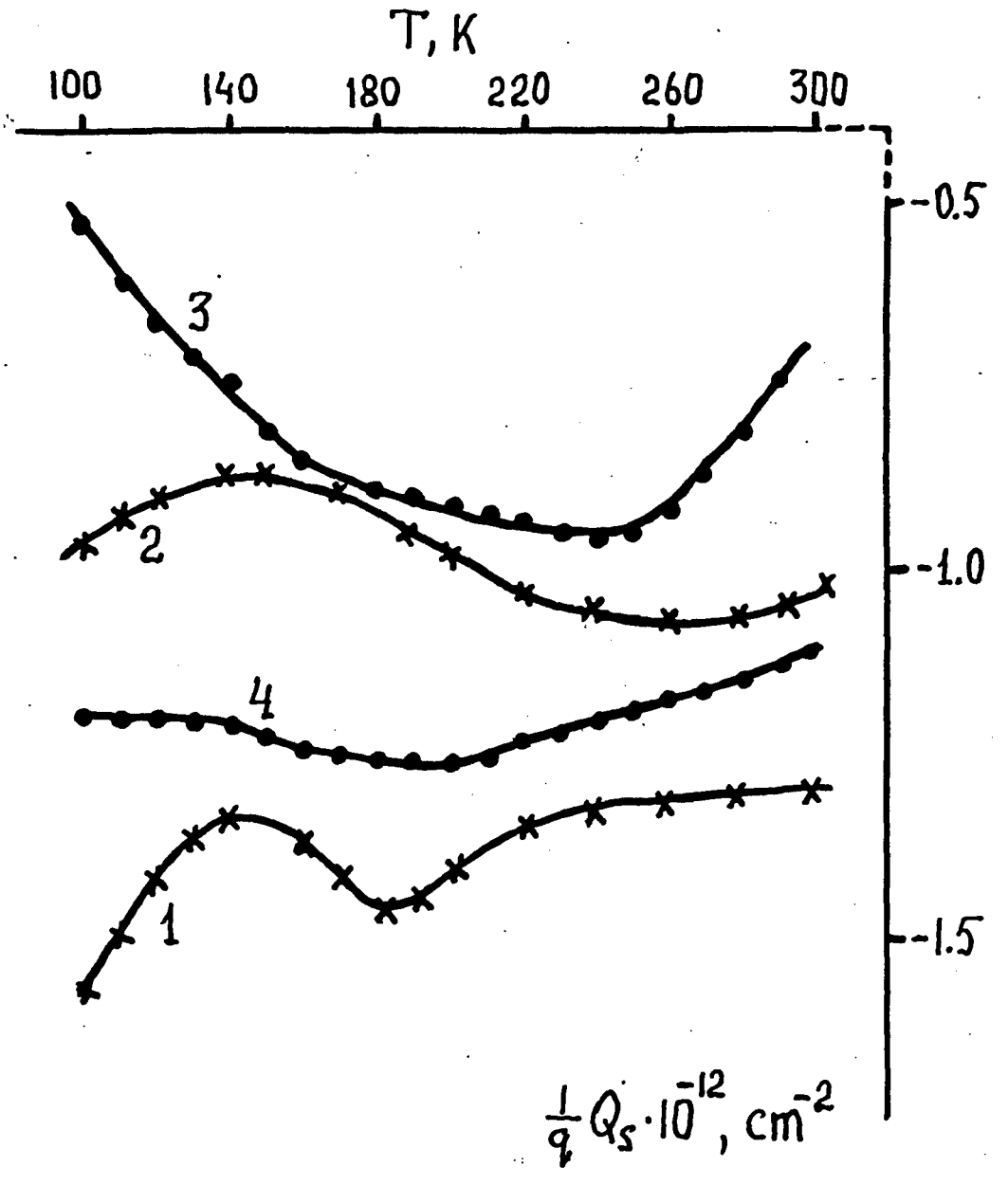

Fig.1.24.Temperature dependencies of the Q_s charge in SES of SiC-6H . 1,2 - (0001) Si surface ; 3,4 - $(0\bar{0}01)$ C surface ; 1,3 - oxidized surface ; 2,4 - surface processed in HF .

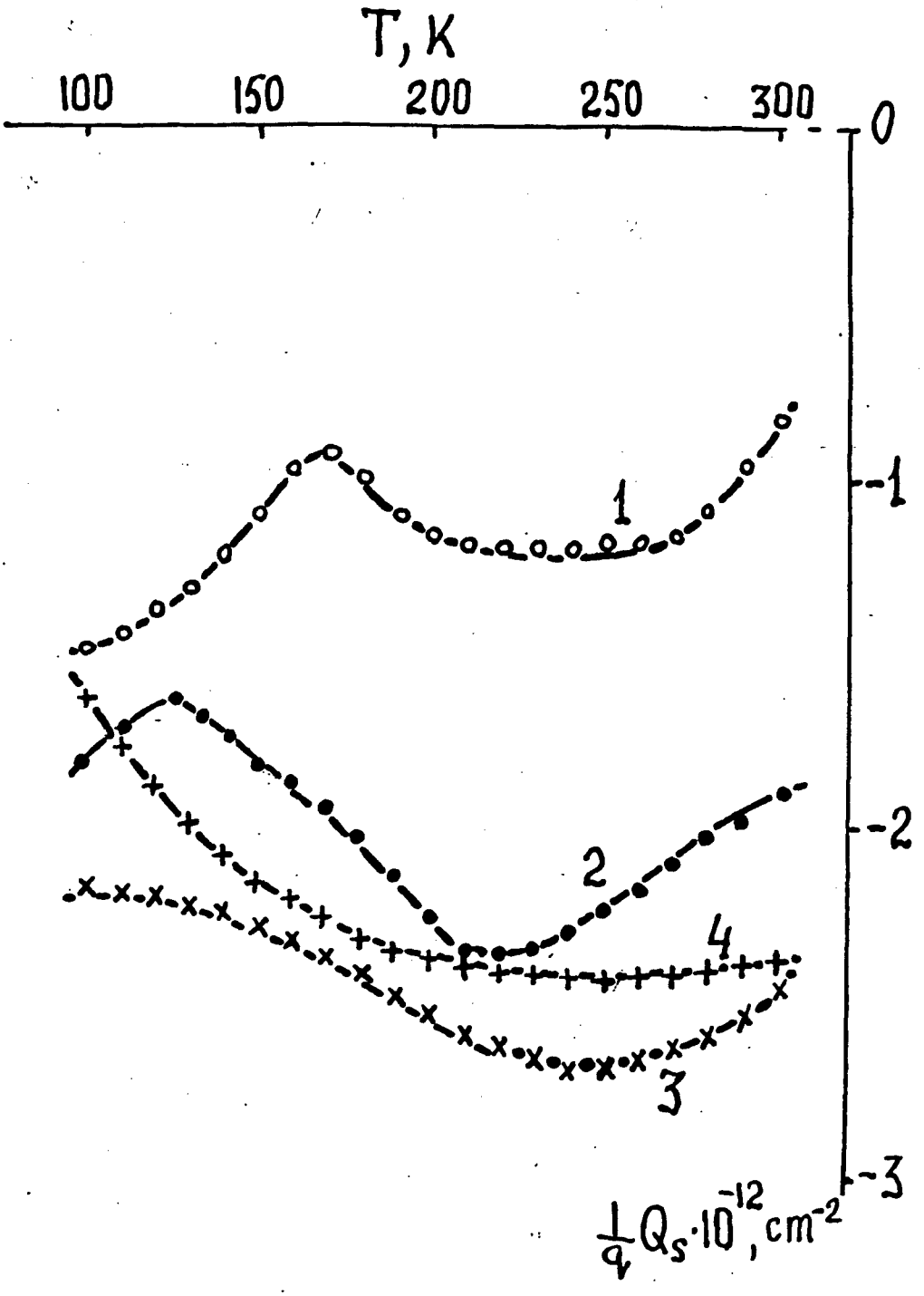

Fig.1.25.Temperature dependencies of the Q_s charge in SES of SiC-15R. 1,2 - (0001) Si surface ; 3,4 - $(0\bar{0}01)$ C surface ; 1,3 - oxidized surface ; 2,4 - surface processed in HF .

of a charge in the fast SES as a function of temperature within the accuracy of a constant charge built in an oxide. As seen from Fig.1.24 and 1.25, the $Q_s(T)/q$ behavior is identical to that of $\phi_{s1}(T)$For the (0001)Si surfaces it has an N-like form, and that for(0001)C is a V-like. For all the $Q_s(T)$ dependencies an increase of a negative charge in SES is characteristic when lowering temperature from 300 down to 240-220 K, which is related, as indicated above, to filling SES with electrons along with the Fermi level shifting to the c band.

In this connection we computed the Fermi level position on a semiconductor surface E_{Fs} and its variation with lowering temperature for various conditions of the (0001)Si and $(0\bar{0}01)$C surfaces of SiC-6H and SiC-15R. It turns out that at 300 K the Fermi level for the (0001)Si surface of SiC-6H, oxidized and processed in HF, is situated by 0.29 and 0.2 eV below the c band.For the same surfaces of SiC-15R it is by 0.1 and 0.21 eV below the c band. The E_{Fs} position on $(00\bar{0}1)$C of SiC-6H is by 0.13 and0.29 eV, respectively, below the c band and that on the (0001)C surfaces of SiC-15R is by 0.33 and 0.32 eV below the c band.With lowering temperature down to 240-220 K the E_{Fs} level position on the surfaces indicated above changes slightly because of a high density of SES. Estimates made for a number of surfaces of SiC-6H and SiC-15R show that the SES density in the vicinity of the Fermi level on these surfaces is within the limits (2 to 10)$*10^{12}$ cm^{-2} eV^{-1}. Below 220-180 K, when one observes in all the cases a decrease of a negative charge Q_s in SES (Fig.1.24 and 1.25), the E_{Fs} level for most of the surface conditions of SiC-6H and 15R approaches considerably to the c band. At minimum values of $|Q_s|$ its position, for example, for the
SiC-15R surfaces characterized by curves 1-4 (Fig.1.25), is,respectively, by 0.07, 0.15, 0.24, 0.15 eV below the c band.

The decrease of a negative charge in SES with the Fermi level E_{Fs} approaching simultaneously to the c band gives evidence that, as already mentioned above, there is a reconstruction of the SES

system occurring with lowering temperature. With such a reconstruction, the SES density below the E_{Fs} level decreases or the density of positively charged SES above E_{Fs} increases. The SES system reconstruction seems to be caused by structural changes at the interface between the silicon carbide crystal and the SiO_2 oxide film covering its surfaces. Reversibility and reproducibility of the $\phi_{s1}(T)$ and $Q_s(T)$ dependencies are indicative of the fact that the structural changes are reversible as well. They may be caused by the elastic stress at the interface SiC-SiO_2 arising from lowering temperature. This can lead, for example, to changing angles between the silicon-oxygen tetrahedrons and in the tetrahedrons themselves situated at the interface, that changes reversibly the fast SES system [33]. The SES system changing,which begins at a certain temperature, gives a V-like behavior of $\phi_{s1}(T)$ and $Q_s(T)$ on the $(0\bar{0}01)C$ surfaces. An N-like behavior of these temperature dependencies on the (0001)Si surfaces covered by non-uniform oxide films is caused by competition of two mechanisms of changing charge: reconstruction of the SES system, when a negative charge in SES decreases, and filling SES with electrons, when it increases with lowering temperature.

3. Now, let us consider the surface potential photomemory effect related to capture of non-equilibrium holes in the surface traps under illumination of the SiC surface. According to that described above, the number of holes captured at a certain temperature. which gives a variation of the potential from ϕ_{s1} to ϕ_{s2}, is equal to:

$$P = [\, Q_{sv}(\phi_{s1}) - Q_{sv}(\phi_{s2}) \,]/q \qquad (1.5)$$

The dependencies calculated using (1.5) for two kinds of conditions for the (0001)Si and $(0\bar{0}01)C$ surfaces of the 6H and15R modification silicon carbide are presented in Fig.1.26 and 1.27,respectively. It is seen that with lowering temperature from 300down to 220 K in all cases the concentration of holes

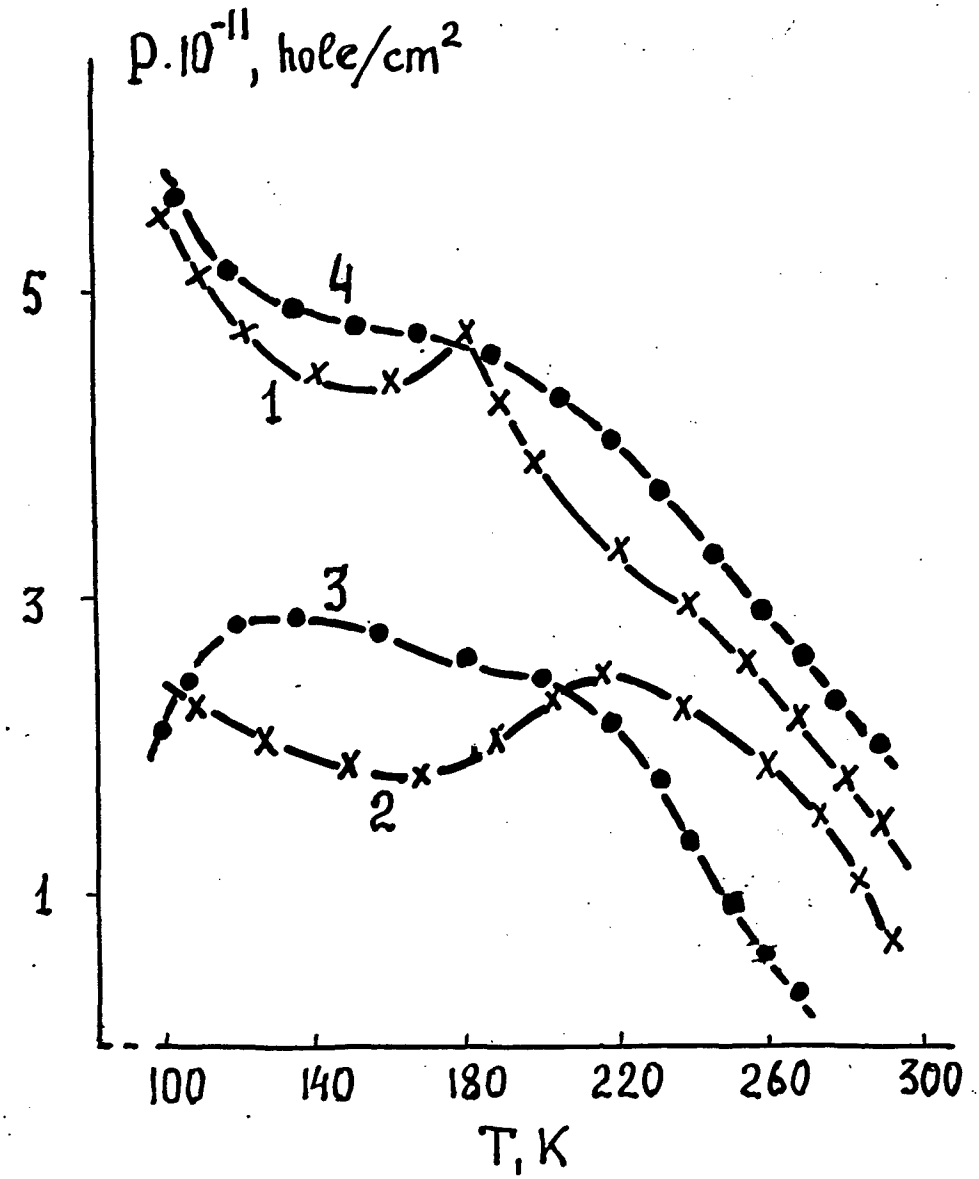

Fig.1.26.Temperature dependencies of the hole concentrations cartured in traps of SiC-6H.1,2 - (0001) Si surface ; 3,4 -(0̄001) C surface ; 1,3 - oxidized surface ; 2,4 -surface processed in HF .

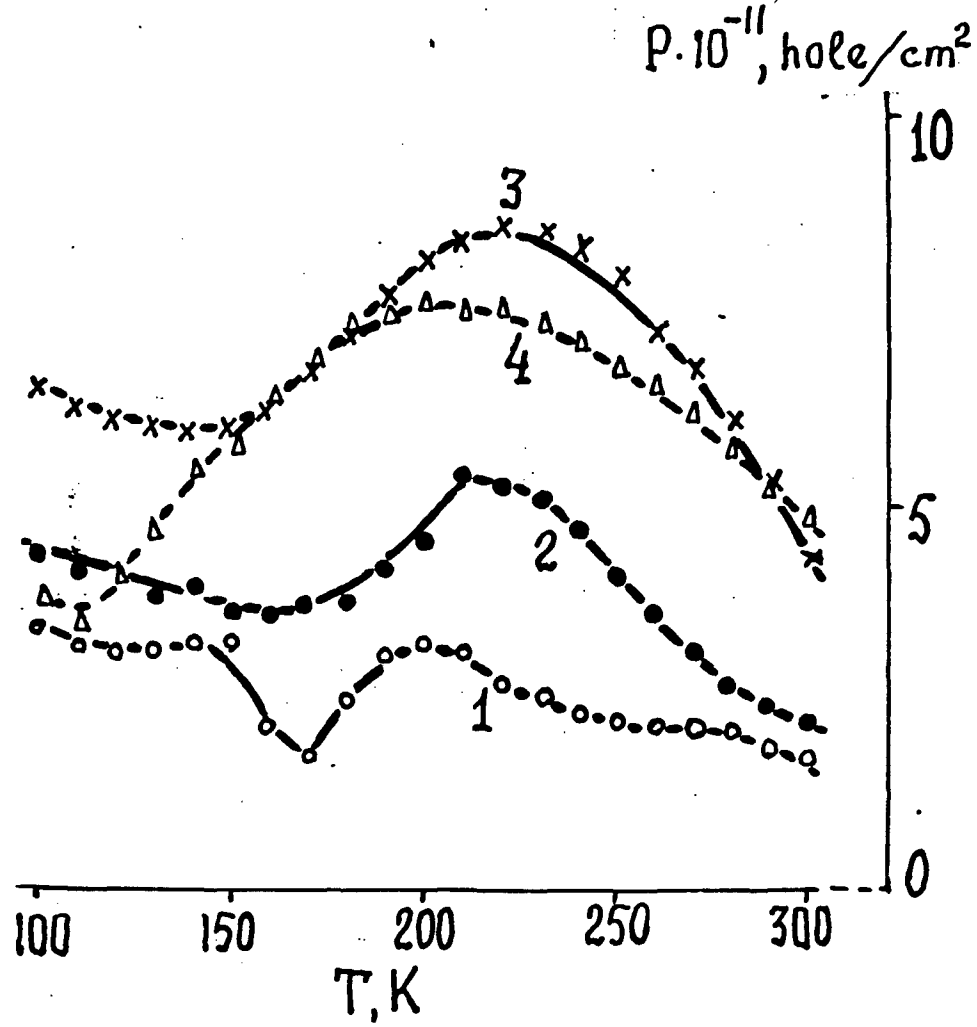

Fig.1.27.Temperature dependencies of the hole concentrations cartured in traps of SiC-15R.1,2 - (0001) Si surface ; 3,4 -(0$\bar{0}$01) C surface ; 1,3 - oxidized surface ; 2,4 -surface processed in HF .

captured in traps increases. Since during the first light pulse action the traps are saturated with holes, then one may state that the P(T) dependence reflects the temperature dependence of the trap concentration for the traps capturing holes. The increasing number of traps, which capture holes with lowering temperature,is related to the fact that there is a set of traps distinguishing by the hole lifetime in them. At higher temperatures the ones manifested as photomemory centers are the traps situated farther from the v-band of SiC. With lowering temperature, because of increasing the time of excitation of holes into the v-band, the traps, which are situated nearer to it, are added to the first ones. Investigations of the photomemory effect relaxation at various temperatures confirm this statement and show that there are several time constants oft his relaxation. Energetic positions of traps estimated from the temperature dependencies of the relaxation time for the charge captured in them overlap the 0.7 eV-wide energetic interval above the silicon carbide valence band.

As seen from Fig.1.26 and 1.27, the number of holes captured and,consequently, the number of traps are maximum (approximately $8*10^{11}cm^{-2}$) at 220 K on the $(0\bar{0}01)C$ surfaces of SiC-15R and they are minimum ones ($\sim 2*10^{11}$ cm^{-2}) on the (0001)Si surface of SiC-6H processed in HF. At temperatures below 220-180 K on the $(000\bar{1})C$ surface of SiC-6H one observes intervals of slowing increase of the trap concentration with lowering temperature (curves 3 and4, Fig.1.26) or even some intervals of decreasing this concentration on the (0001)Si surface of SiC-6H (curves 1 and 2,Fig.1.26) and on all the SiC-15R surfaces (Fig.1.27). In this case the P(T)-dependencies for the (0001)Si surfaces of SiC-6H and 15R have an N-like behavior.As following from the $\Phi_{s1}(T)$ dependencies, this is the very temperature region where the reconstruction of the SES system occurs for the states situated in the upper half of the SiC energy gap. Therefore, one may conclude that the traps capturing holes have a nature of origin which is common with that of SES and they differ from the latter only by the larger cross-section of

hole capturing. The structural reconstruction at the interface between a semiconductor and an oxide film occurring with lowering temperature changes the SES parameters including those states,which manifest themselves as traps for non-equilibrium holes.

47

II Section

AVALANCHE LIGHT EMITTIING DIODES

Avalanche light emitting diodes (LEDs) are semiconductor devices using optical emission which arises in the p-n-junction under the avalanche breakdown. Such LEDs are characterized by a wide emission spectrum from 200 to 2500 nm , high temperature and temporal stability of emission, and their speed is limited by technical potentialities of modern electric pulse generators of the subnanosecond range. In connection with availability of these useful properties the avalanche LEDs may be used as reference emission sources to check stability of photoreceiving tracts, as sources of subnanosecond light pulses, as sources of UV emission as well as to imitate emission of space objects in astronomy and astronautics.

2.1. Investigation of parameters and technology .

Under the conditions of reverse bias an electric field in the p-n-junction easily achieves values of 10^5 to 10^6 V cm^{-1} in such fields, as a rule, the electric breakdown of the p-n-junction takes place, which is accompanied by sharp increase of a current and emission of photons. The emission spectrum of SiC diodes overlaps a wide range of photon energy and for this reason it differs from those corresponding to other electroluminescence mechanisms (Fig.2.1).

In the case, when the effects of selfabsorption can be made negligible, the emission is in fact independent of the concentration and given impurity composition in a crystal,and it is also slightly sensitive to variation of temperature [34].

Investigations show [34] that a wide-band structureless emission is caused by the intraband non-direct transitions of high-energy carriers. High-energy carriers are capable to excite also the recombination luminescence bands. However, these bands

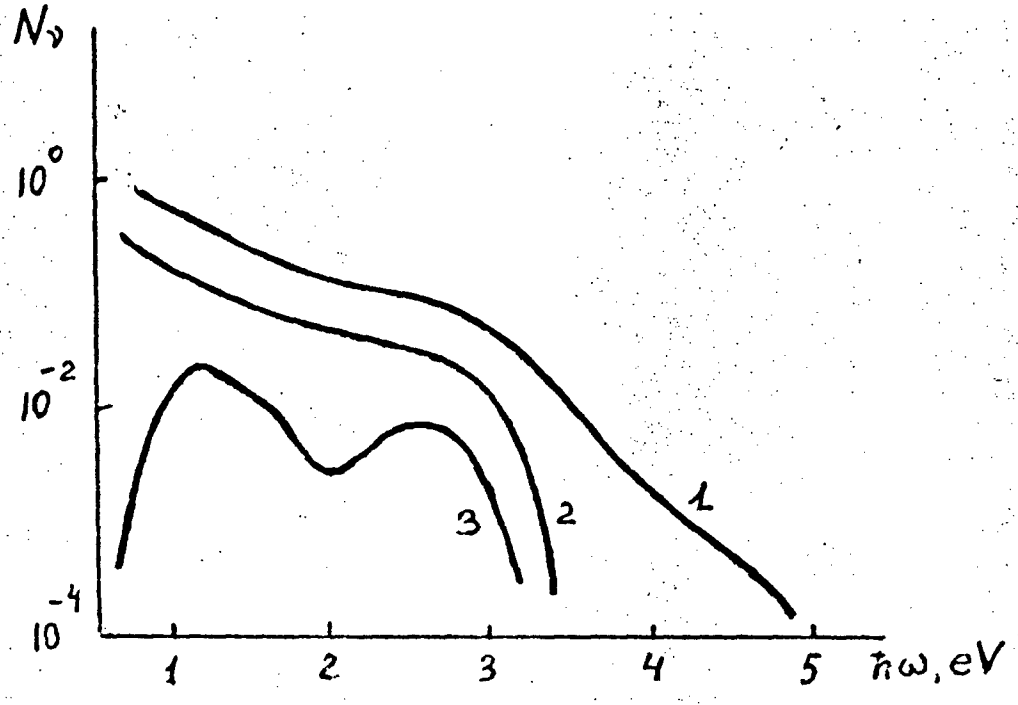

Fig.2.1.Emission spectrum of LEDs based on SiC
1 - LED with "open" design ; 2,3 - LEDs with "closed" design and uncompensated donor concentration : 2 - 2×10^{17} cm^{-3} ; 3 - 3×10^{16} cm^{-3} .
Y - axis : N_ν arb. units .

are superimposed on the continuous spectrum and may manifest themselves as some structure on the background of this spectrum.

The technology of avalanche LEDs has a number of peculiarities. Used for their fabrication are the 6H- and 15R-SiC crystals of n-type with the uncompensated donor concentration of (0.5 to 6)$*10^{18}$ cm^{-3}. In the case of fabrication of p-n-junctions using customary methods (diffusion, epitaxy, MIS-technology) the breakdown voltage varies within the limits (0.3 to 2)$*10^{2}$ V. Application of the alloying technique enables to decrease the breakdown voltage down to (15 to 30) V and to fabricate fast LEDs with a small area [35,36]. However, use of such junctions has a number of shortcomings: small number of microplasmas (MP) and large spread by the breakdown voltage of individual MPs in the same p-n-junction. As a rule, these microplasmas are situated in the peripheral and widely spaced parts of p-n-junctions.

Authors of [37-40] have developed an improved alloying technique for fabrication of LEDs with a small area $S<10^{-4}$ mm^2. It consists in a preliminary treatment of crystal surface with a view to obtain p-n-junctions with a large quantity of microplasma regions with nearly identical breakdown voltages.

Fig.2.2 and 2.3 present typical reverse-bias I-V characteristics of the diodes and their dependence of the differential resistance on the reciprocal current (1/I). Analysis of the characteristics enables to distinguish the following four parts:

1. In the region of small currents 10^{-7} A (10^{-3} A/cm^2)< I < 10^{-5} A (10^{-1} A/cm^2) one observes, as a rule, a linear dependence of the current on the voltage.

2. In the region of 10^{-5} A (10^{-1} A/cm^2) < I < 10^{-3} A(10 A/cm^2) the tunneling breakdown is predominant. This part manifests itself in the most LEDs and it is characterized by a linear dependence of the differential resistance on the reciprocal current (1/I).

3. Intermediate region: 10^{-3} A (10 A/cm^2) < I < 10^{-2} A(100 A/cm^2). Current flowing in this region is caused by simultaneous

Fig.2.2.Current voltage characteristics of the diodes with breakdown voltage : 1 - 21.6 V ; 2 - 21.2 V ; 3 - 20.02 V ; 4 - 19.05 V ; 5 - 17.99 V ; 6 - 17.12 V .

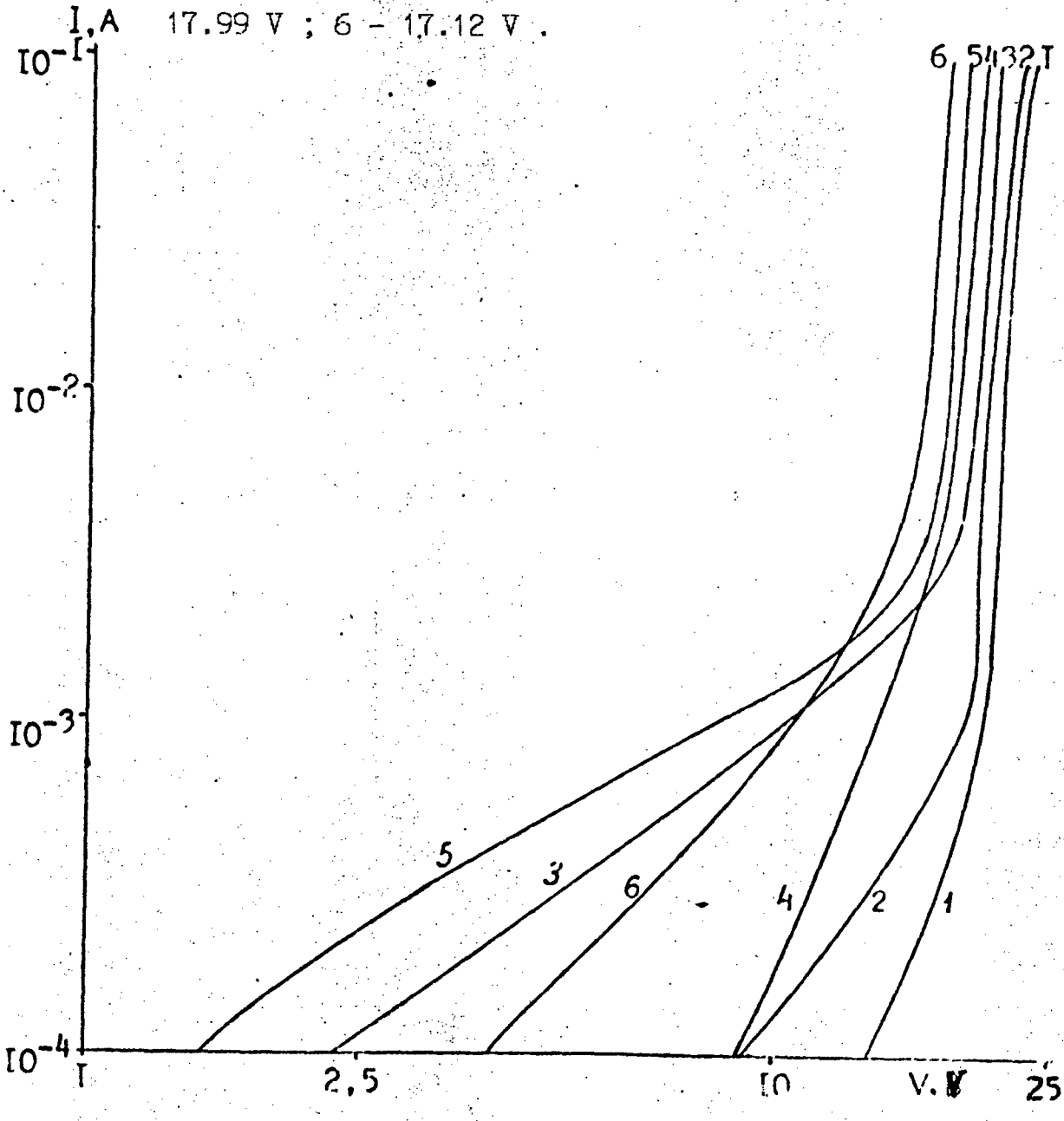

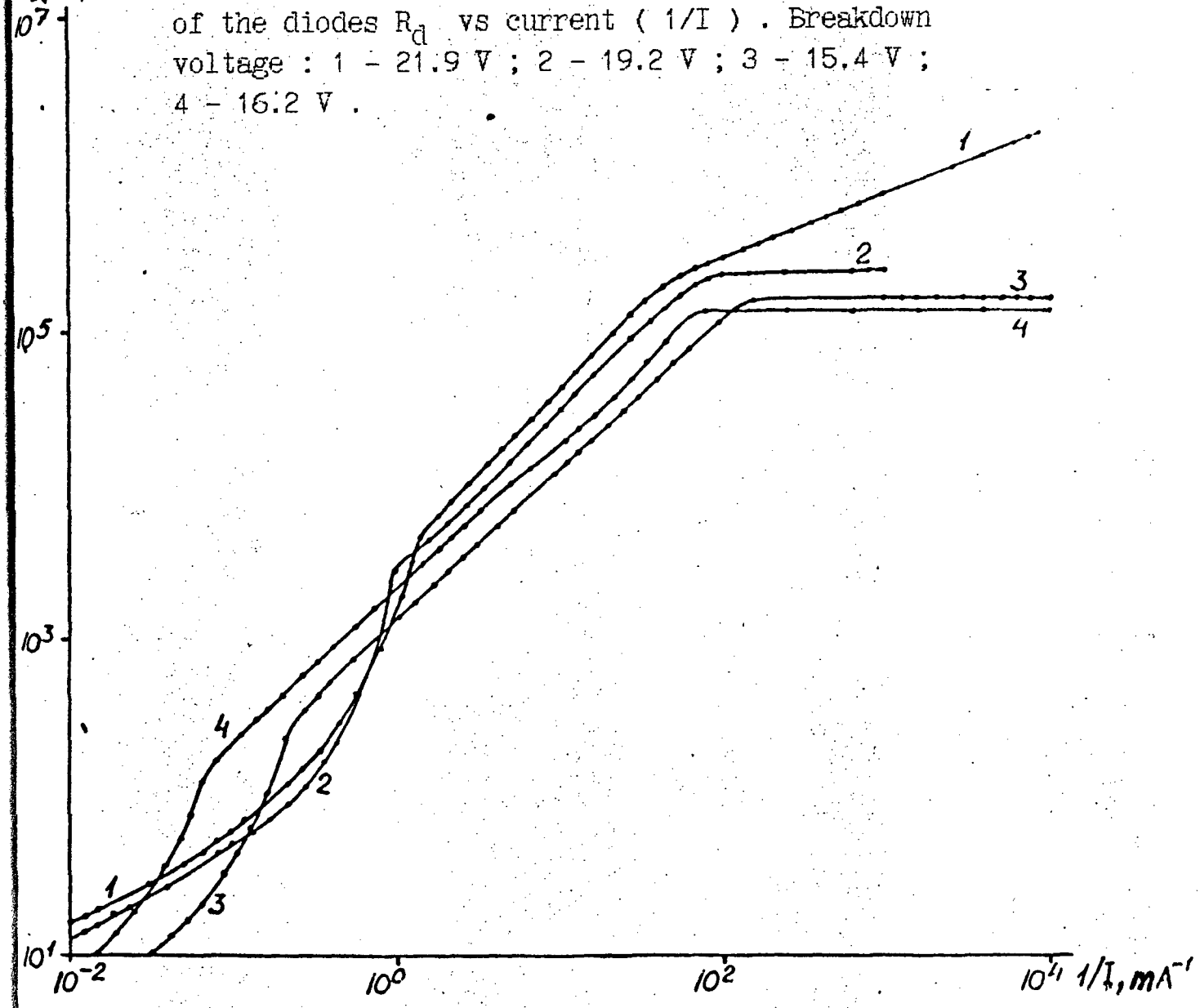

Fig.2.3.Dependence of the differential resistance of the diodes R_d vs current (1/I) . Breakdown voltage : 1 - 21.9 V ; 2 - 19.2 V ; 3 - 15.4 V ; 4 - 16.2 V .

action of the tunneling effect and impact ionization.

4. High current density region: I> 10^{-2} A (100 A/cm^2). In this region the I-V characteristics are described by the expression indicative of the avalanche breakdown:

$$I= (U - U_{br})/ R_d$$

The differential resistance value R_d as a function of the breakdown voltage 16 to 30 V varies within the limits from 8 to 30 Ohm. As following from these investigations the LED equivalent circuit may be presented as shown in Fig.2.4.

Fig.2.5 presents the dependence of the emission intensity on the current. One may distinguish two typical parts. At high current densities under the conditions of avalanche breakdown we have P~I, i.e. in this regime the quantum yield of emission is independent of the current. In this case difference in the external quantum yield of LEDs with different breakdown voltages is mainly caused by absorption of emission during its leading-out through a crystal. LEds with high breakdown voltages (material with a lower uncompensated donor concentration) have a higher external quantum yield.

In the intermediate current region ($P \sim I^n$, where $1<n<2$) the quantum yield is 2 to 3 times as low than that in the avalanche breakdown region and it increases with increasing current.

The LED characteristic of importance is their long-term stability of parameters, especially of emission intensity. We have developed the special automated stand [6] to measure this important parameter. The main idea of the method consists in comparison of the emission intensity of the LEDs under study and that of reference sources. At the same time it is assumed that the emission intensity variation for reference sources (long-term instability) is small and does not exceed some known value. Such a concept of measurements enables to eliminate instability of a photodetector transfer function. A set of the radioluminescent

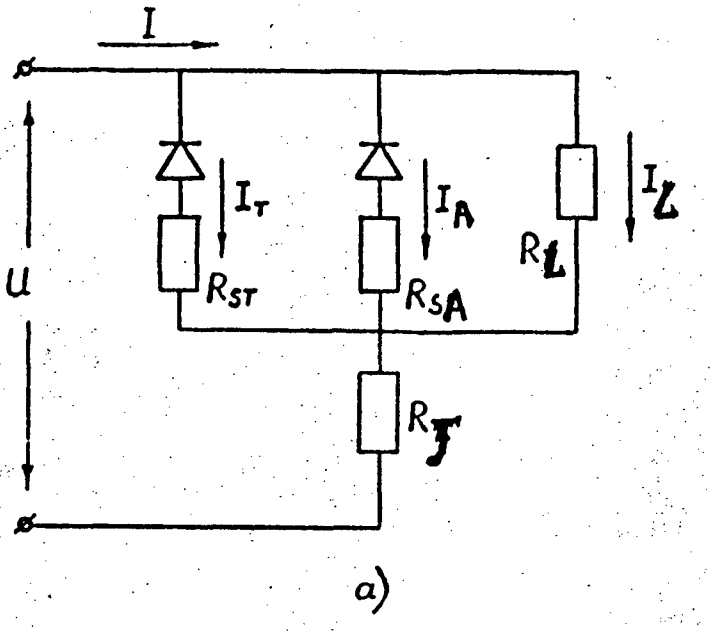

a)

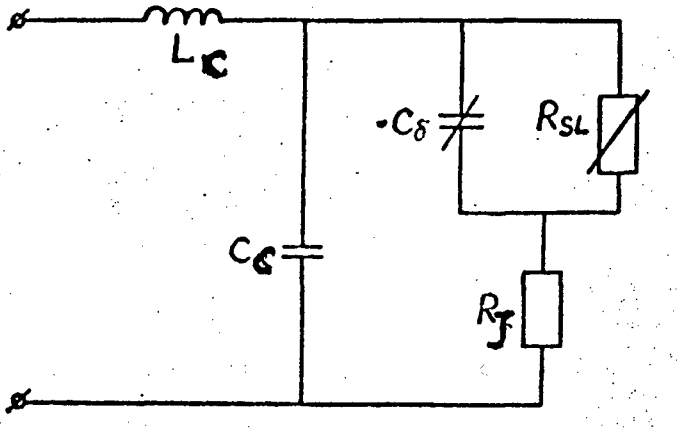

б)

Fig.2.4.Equivalent circuit of LED for : a - direct current ; b - high frequency supply . Here I_T,R_{ST} - tunnel components of spilling current and resistance; I_A,R_{SA} - avalanche components ; R_L , R_J and R_{SA} - leakage resistance , junction resistance and series avalanche resistance respectively of the avalanche breakdown ; L_C,C_c - reactances of a can .

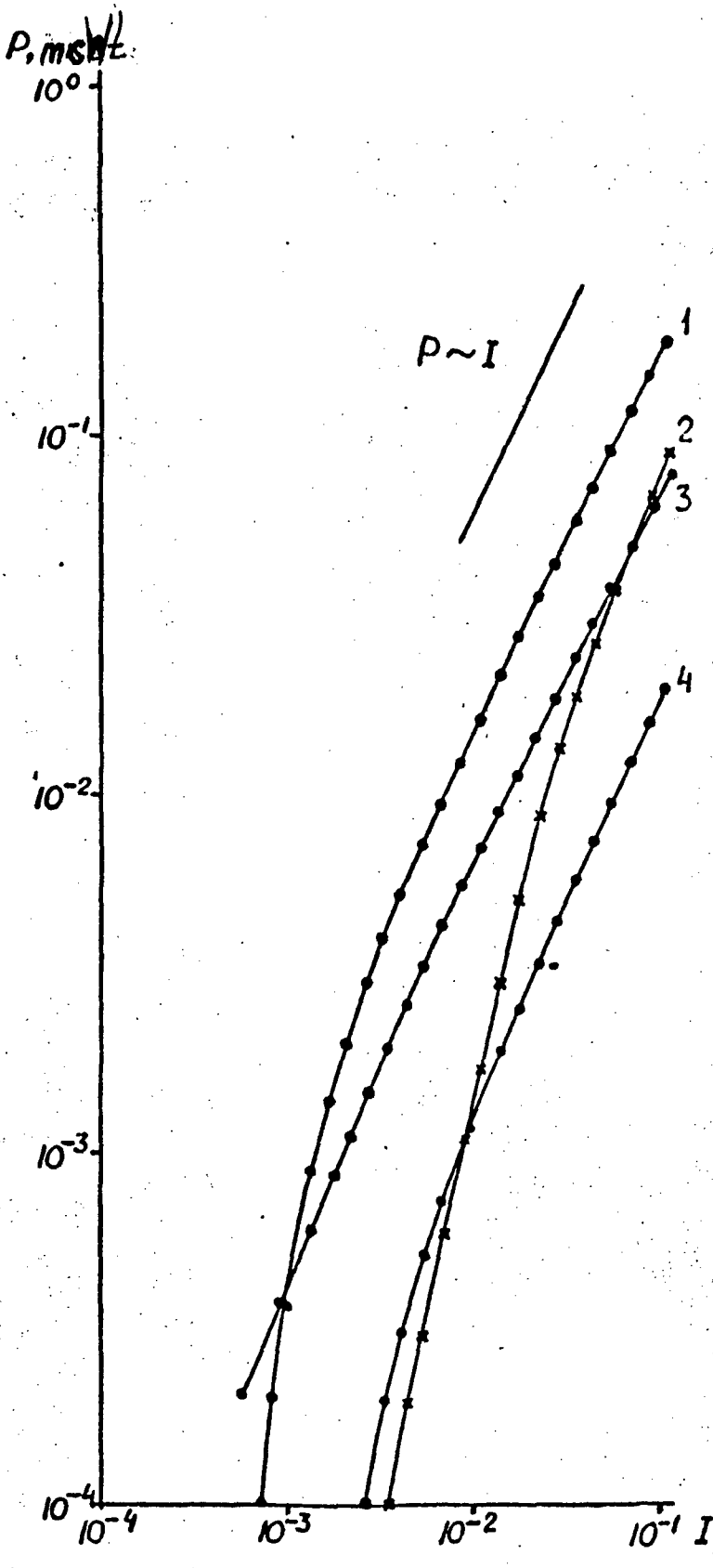

Fig.2.5.Dependence of the emission intensity vs current for LEDs with breakdown voltage : 1 - 27.5 V ; 2 - 16.9 V ; 3 - 19.2 V ; 4 - 15.4 V .

emitters (RLE) based on a mixture of a crystallophosphor with a radioactive substance containing C^{14} is used as reference sources. The temporal instability of the reference sources was no more than $5.7*10^{-6}$ h^{-1}. Measurements were carried out using a photomultiplier in the photon-counting regime. The measurements carried out for a group of three RLE and six avalanche LEDs have shown that both kinds of sources with a high accuracy are described by the Poisson distribution and LEDs after preliminary training have a high long-term stability of emission, which is no more than 3 % per 1000 h of operation.

Measurements of the avalanche LED speed were carried out in the Institute of Physics of Solids at Latvian State University . We made use of the single-photon statistical method with the time resolution of 0.25 ns and the subnanosecond generator shown in Fig.2.6.

Fig.2.6 shows a light pulse from the avalanche LED. The pulse duration at half height is no more than 0.5 ns at the 0.2 level of amplitude - no more than 0.7 ns. The pulse decay is exponential with the time constant of 0.15 ns within the limits of than 3 decimal orders. The dynamical range of measurements is 4 orders of magnitude and it is limited a photomultiplier interference.

The physical limit of speed for our LEDs cannot be determined at present because of insufficiently high level of the subnanosecond equipment. Further decreasing the light pulse duration may be possible after improving the pulse generator design.

2.2. Technical parameters

- spectral emission range (*)		200 to 2500 nm
- flash intensity at the 1 ns duration (photon number, no less)		5000
- temperature coefficient of emitted intensity (no more)		0.1 %/degree
- time constant (no more) (**)		0.2 ns
- emission zone diameter		30 to 150 μm
- operation temperature range (***)		-60 to +80 °C
- operation voltage range:	dc	18 to 30 V
	pulse current	up to 100 V
- operation current range:	dc	up to 150 mA
	pulse current	up to 10 A (****)
- operation life (no less)		100000 h

(*) the spectral range is indicated for the "open" design;

(**) resolution limits of the measuring set-up;

(***) determined by a capsule design; fabrication of LEDs with a wider range is possible;

(****) permissible limits of the pulse current are determined by the pulse duration; for short pulses T<3 ns I_{max}=10 A, at T <10ns I_{max}=3 A.

Figures below present the LED design (proposed to a customer). There is a possibility to apply other design versions coordinated with a customer.

By their electrical characteristics and operation principle the avalanche LEDs are similar to the semiconductor voltage-reference diodes.Therefore they work under a reverse bias Note: in the case of direct current supply the LED device must be mounted on a radiator with an effective area corresponding to the power dissipated by LED (~3 W). For the design versions presented here the polarity of power supply corresponds to positive voltage on a can. In the pulse operation regime LEDs can be used without radiators in case the mean dissipated power is no more than 100 mW. With the pulse duration

T>10 ns the maximum pulse current should be no more than 200 mA. In the case of short pulses T<3 ns the current may reach 10 A.

Parameters of fabricated LEDs

No.	Design	V_{br},V	R_{dif}(I=100 mA) Ohm	P(450-600 nm) mcWt
505	"Closed"	20.52	18.44	0.129
532	"	21.06	16.01	0.135
610	"	20.75	11.65	0.160
630	"	21.25	16.02	0.152
641	"	20.86	15.05	0.141
649	"	23.23	16.51	0.167
673	"	22.42	16.96	0.157
674	"	22.40	15.00	0.149
684	"	27.32	25.63	0.158
1	"Open"	20.50	10.00	
2	"	19.80	15.00	

The light emitting diodes of given design have been tested and are applied in the Institute of Physics of Solids in the Latvian State University, Institute of Nuclear Physics (SDAC, Novosibirsk), Physical Institute (PIAN, Moscow), Institute of Theoretical and Experimental Physics (ITEP, Moscow).

Section III

HIGH-TEMPERATURE THERMAL RESISTORS BASED ON SILICON CARBIDE

The modern industry needs in temperature sensors which are capable to operate under the conditions of high temperature and aggressive media. Such demand, in particular, exist for semiconductor thermal resistors. They gain interest in them first of all due to high sensitivity as compared to the wire-type thermal resistors and thermocouples. Yet, devices based on customary semiconductor materials cannot work under extreme conditions. The most attractive material for this purpose is silicon carbide. It is caused first of all by its thermal and chemical durability and a wide band gap. Moreover, the silicon carbide devices are characterized by a high performance stability. Many laboratories in various countries exert every effort to develop technology of thermal sensors based SiC. It is customary to use for this purpose either single crystals doped with boron or thin films on the insulating substrata prepared by the RF plasma sputtering. Such thermal resistors distinguish by their high stability and relatively low extreme operation temperature [41-44].

In this connection we exert an effort to develop technology to fabricate cheap thermal resistors for a wide temperature range.

3.1. Thermal resistors based on the polycrystalline SiC

The method of synthesis from the separate Si and C sources had been used for fabrication of the polycrystalline SiC. The synthesis proceeded on surface of a graphite substrate. At the synthesis temperature (1800 to 2000 ^{o}C) the cubic modification SiC (3C-SiC) was formed, as a rule. To provide uniformity of the SiC layer along the structure depth, we have developed the rig with special design, which provides desired distribution of temperature over the operation space. The SiC layer deposition rate was up to

0.2 to 2.0 mm/h. It was possible to obtain layers up to 10 mm thick. The method productivity is determined by the graphite rig dimensions and, consequently, furnace dimensions. For example, the improved set-up "Редмет-30" during a technological cycle provides fabrication of material for 50 to 100 thousand thermal resistors. The material has the n-type conduction. Investigations of the material structure has shown that the SiC layers directly adjacent to the graphite substrate are, as a rule, fine-grain and in fact textureless. The grain growth direction in regard to the substrate is determined by the flux direction of vapors: Si, SiC, SiC_2 and Si_2C, and, consequently, it depends on the furnace rig design. With thickening the film a pillar-like shape of grains is manifests explicitly itself. The maximum cross-section size of grains is 250 to 500 mu .

Having grown SiC we removed the graphite substrate by burning it in air. Using the diamond disk saw we cut flat plates with a desired shape. The plate surface was processed using diamond pastes.

To obtain high-temperature thermal resistors with high sensitivity one needs the material conduction to be determined by an impurity with a high energy of thermal activation. For SiC such an impurity is boron (E_i=0.39 eV). The diffusion coefficients of impurities in SiC are small. Therefore, in order to dope a single crystal over the entire volume, high temperatures and rather long time are needed. Application of the polycrystalline SiC gives new potentialities for fabrication of thermal resistors. When doping this material, boron easily penetrates in interstitials between microcrystals and diffusion proceeds in fact simultaneously from the entire surface. As a result, the p-n-p structure is formed in every microcrystal. Thus, the thermal resistor consists of a series chain of microcrystals and p-n-p, p-n-p,...,p-n-p structures. Such an arrangement provides high resistivity of material and its high thermal sensitivity. The diffusion procedure was carried out by known technique at the temperature 1800 ^{o}C in the argon medium, 100 to 200 tor. A diffusant was the boron oxide.

Fig.3.1 presents typical I-V characteristics of the thermal resistors. It is seen that they are linear in the small current region. Current increasing leads to increasing the power dissipated by a thermal resistor. Already at $P>2*10^{-6}$ W the I-V characteristic deviates from its liner law. It seems that this is caused by self-heating of thermal resistors. In order to investigate what causes this deviation, we measured the I-V characteristics in various media: in oil, in air and in vacuum. As seen from comparison of curves 3 and 4 in Fig.3.1, sample self-heating takes place indeed. Fig.3.2 illustrates variation of resistance for a typical sample as a function of the air pressure under the conditions of constant current through a resistor.

$$\delta R = \frac{R_o - R}{R_o} 100\% \qquad (3.1)$$

R_o is the sample resistance at $I=I_{meas}$ under the standard conditions. As seen from this Fig.3.2, the thermal resistors based on SiC may be applied as sensitive sensors of vapor/gas pressure.

Fig.3.3 presents typical temperature dependencies of the thermal resistor resistance. As it is seen, they are well described by

$$R = R_o*\exp(B/T) \quad \text{or} \quad R \sim \exp (E_i/kT) \qquad (3.2)$$

where B=4500 and E_i=0.39 eV, which corresponds the thermal activation energy of boron.

3.2. Thermal resistors based on bulk crystals of SiC

The thermal resistors have been fabricated by the radiation method of doping the 6H-SiC single-crystals with subsequent processing [45,46]. Such technology enables to obtain material with high resistively (10^{12} to 10^{14} Ohm cm), with a high thermal activation energy ($E_1>0.9$ eV), and high sensitivity. Its

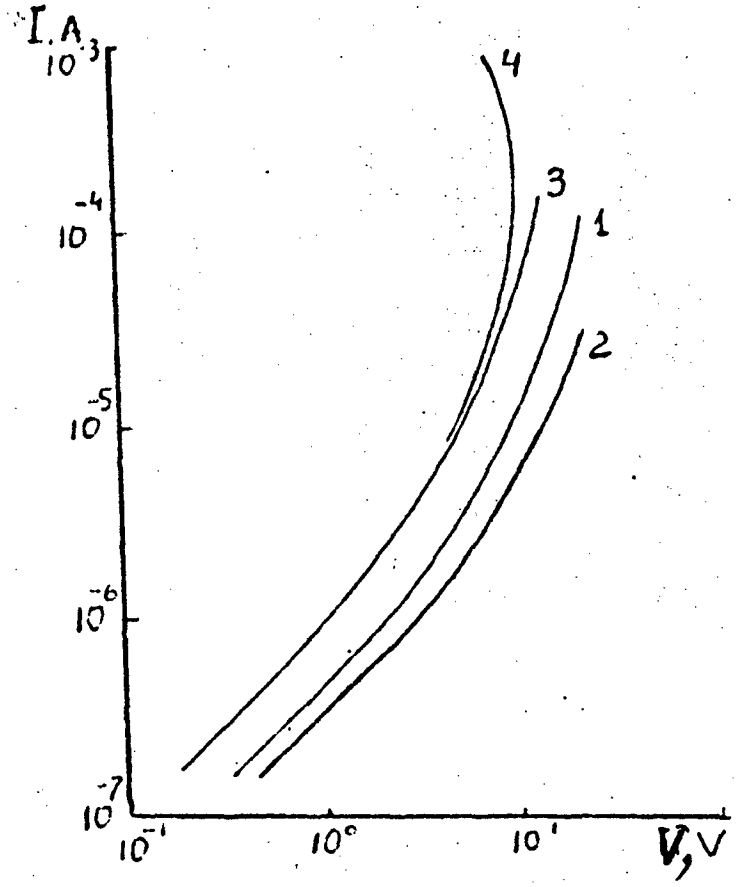

Fig.3.1.Current voltage characteristics of thermal resistors . 1,2 - samples No 211 and 12 respectively measured in air under the standard conditions ; 3 - sample No 284 measured in vacuum oil ; 4 - sample No 284 measured in vacuum $\approx 10^{-2}$ torr .

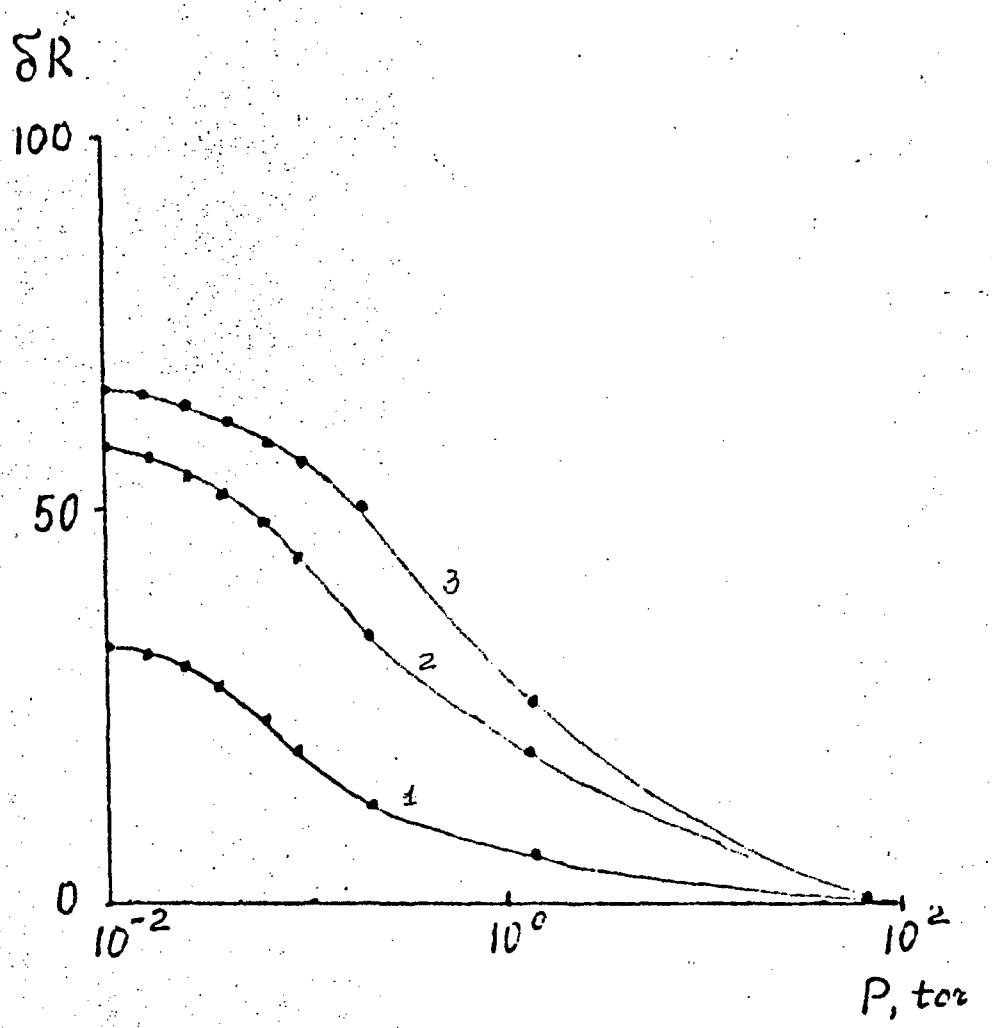

Fig.3.2.Dependence δR vs air pressure at constant current through the thermal resistor for three samples .

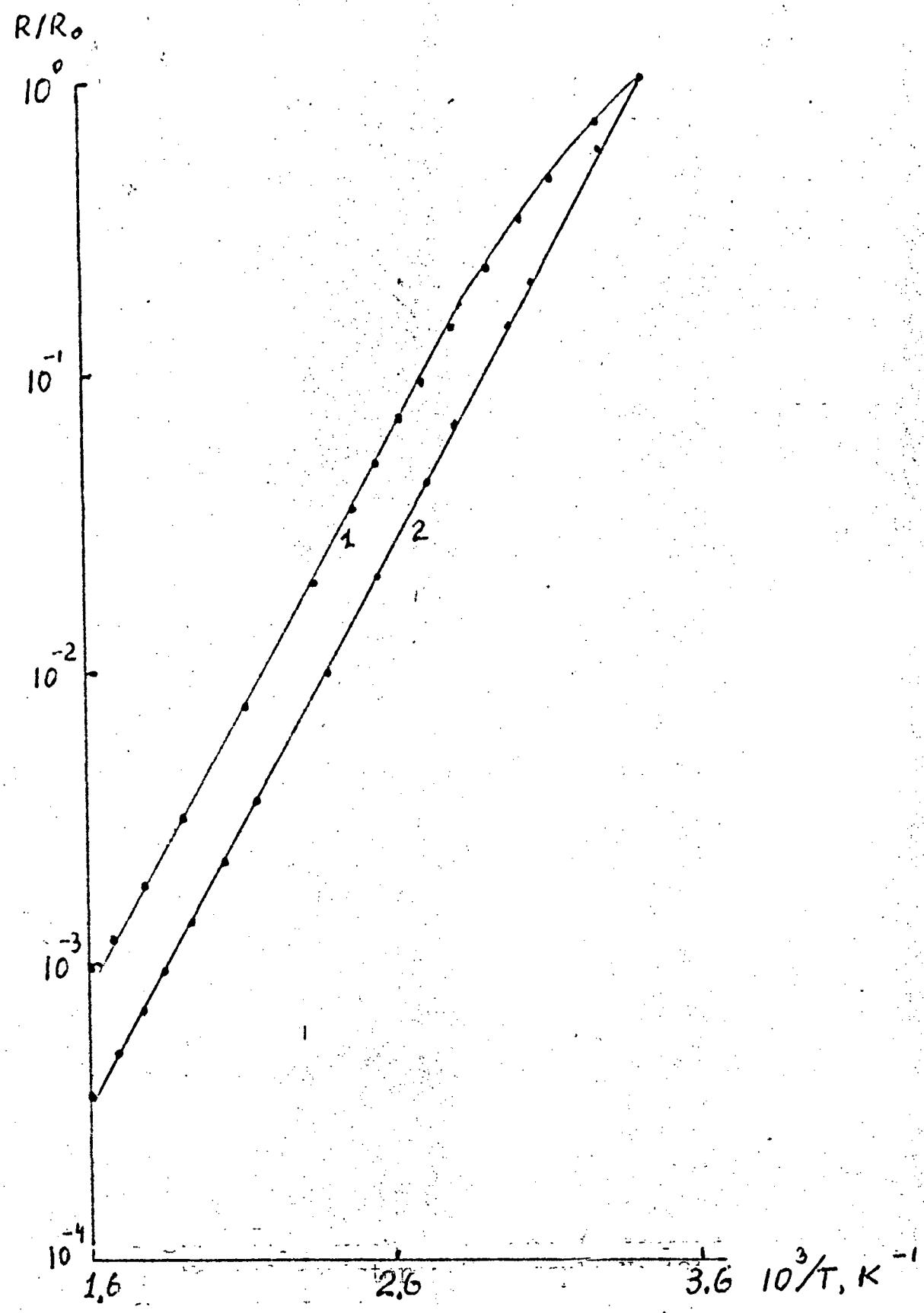

Fig.3.2.Dependence resistance vs temperature of thermal resistor : 1 - sample No 121 ; 2 - sample No 213 .

temperature dependence of resistivity is described by expression (3.2) with B=10000.

Main parameters
Main Technical Characteristics

Parameter	Thermoresistor type	
	polycrystalline	single-crystalline
Available range of R_o at temperatures, C deg. 20 200	100 kOhm to 10 MOhm	100 kOhm to 100 MOhm
Operation temperature range, C deg.	20 to 600	200 to 800
Val. of B in Eqn.(3.1)	4500	10000

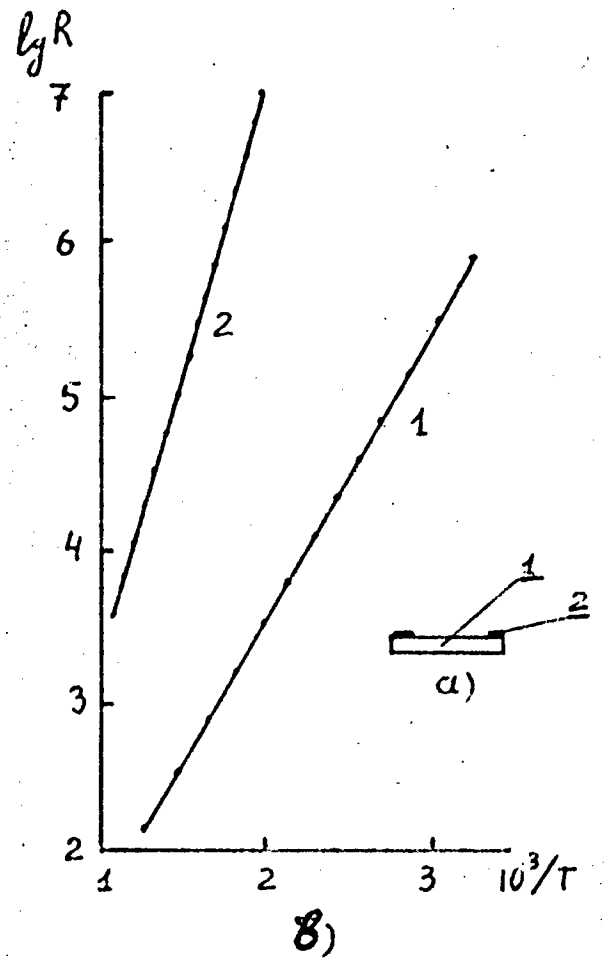

Fig.3.4. a)Arrangement of thermoresistors :
1 - SiC crystal , 2 - Ni contacts .
b)Resistance vs temperature dependencies :
1 - polycrystalline sample ; 2 - single-crystalline sample .

REFERENCES

1.J.A.Lely. "Darstellung von Einkristallen von Siliciumcarbid und Beherrdchung von Art und Menge der eigenbanten Verunreinigungen", Ber. Dt. Kerm. Ges., vol.32, pp.229-231, 1955.

2.Y.M.Tairov and V.F.Tsvetkov, "Investigations of growth processes of ingots of silicon carbide single crystals". J.Cryst.Growth, vol.43, pp.209-212, 1978.

3.V.J.Levin, Y.M.Tairov, M.G.Travadzhyan and V.F.Tsvetkov, "Growing monocrystalline bars of SiC from the gas phase". Inorganic Mat., vol.14, pp.830-83, 1978.

4.Y.M.Tairov and V.F.Tsvetkov. "General principles of growing large-size single crystals of various silicon carbide polytypes". J.Cryst.Growth, vol.52, pp.146-150 , 1981.

5.L.Hoffmann, G.Ziegler, D.Theis and C.Wegrich, "Silicon carbide blue light emitting diodes with improved external quantum efficiency", J.Appl.Phys., vol.53, 6962-6967, 1982

6.G.Ziegler, P.Lanig, D.Theis and C.Wegrich. "Single Crystal of SiC Substrate Material for Blue Light Emitting Diodes". IEEE Transactions on ED, vol.ED-30, No.4, 277-281,. 1983.

7.T.Nakata, K.Koga, Y.Matsushita, Y.Ueda and T.Niina. "Single crystal growth of 6H-SiC by a vacuum sublimation method, and blue LEDs". In book: Springer Proced. in Phys., vol.43, 1989, p.26-34.

8.R,.A.Stein, P.Lanig, S.Leibenreder. "Influence of surface energy on the growth of 6H- and 4H-SiC polytypes by sublimation". Mat.Science and Engin. vol.B11, 69-71, 1992.

9.K.Koga, T.Nakata and T.Niina. Ext. Abstr. 17th Conference SSDM, 249, 1985.

10.S.F.Avramenko, V.V.Vainberg, E.F.Venger, S.I.Kirillova, V.S.Kiselev, V.E.Primachenko, O.T.Sergeev. "Electric and optical properties of the cubic modification polycrystalline silicon carbide". Optoelektronika i Poluprovodnikovaya Tehnika, 1994, No.28, pp.28-33 - in Russia .

11.A.J.R. Lang - Acta Crystallogr. 1959, v.12, p.249.

12.I.L. Shulgina - Author's abstract of Thesis (doctor of sciences, physics & mathematics), Leningrad, 1985 - in Russia.

13.A. Jenkinson ,A. Land in: "Direct methods of investigation of defects in crystals", Moscow, "Mir" Publishers, 1965.

14.D.W.Feldman,J.H.Parker,W.Choyke,L.Patrick - Phys.

Rev.,1968,v.173,N3,p.787.
15.V.I.Levchuk,B.F.Tsvetkov,M.A.Chernov - Kristallografia, 1982,v.27,N3,p.610 - in Russia .
16.E.N.Kalabukhova,S.N.Lukin,B.D.Shanina,L.V.Artamonov, E.N.Mokhov, Sov.Phys Sol. State 32, 482 (1990)
17.E.N.Kalabukhova, N.N.Kabdin,S.N.Lukin, E.N.Mokhov, B.D.Shanina, Sov.Phys Sol. State 31, 378 (1989)
18.M.V.Alekseenko, A.I.Veinger, A.G.Zabrodskii, V.A.Il'in, Yu.M.Tairov, V.F. Tzvetkov, JETP Lett. 39, 304 (1984)
19.A.I.Veinger, Phys. and Techn. Semicond. 8, 70 (1969)
20.S.Maekawa, N. Kinoshita, J. Phys. Soc. Jap. 20, 1447 (1965)
S.F.Avramenko,E.F.Venger,S.I.Kirillova,V.S.Kisilev, V.E.Primachenko - Poverhnost,1993,N6,p.89 .
21.S.F.Avramenko,V.V.Vainberg,E.F.Venger,S.I.Kirillova, V.S.Kisilev,V.E.Primachenko,V.A.Chernobai- Fizika i Tehnika Poluprovodnikov,1994,N6,p.989.
22.S.F.Avramenko,E.F.Venger,S.I.Kirillova,V.S.Kisilev, V.E.Primachenko - Ukr.Fiz. Jurnal,1993,N2,p.268 .
23.Silicon carbide (structure, properties and application field). ed. by I.N.Frantsevich, Kiev, 1966.
24.A.V.Sachenko, O.V.Snitko. Photoeffects in surface layers of semiconductors. Kiev, 1984.
25.V.E.Primachenko, O.V.Snitko. Physics of semiconductor surface doped with metals. Kiev, 1988.
26.S.I.Kirillova, V.E.Primachenko, O.V.Snitko, V.A.Chernobai. Poverhnost, No.12, 85 (1990).
27.S.I.Kirillova, V.E.Primachenko, O.V.Snitko, V.A.Chernobai. Optoelektronika i Poluprovodnikovaya Tehnika, No.20, 15 (1991).
28.S.I.Kirillova, V.E.Primachenko, V.A.Chernobai, O.V.Snitko. Poverhnost, No.11, 74 (1991).
29.S.I.Kirillova, V.E.Primachenko, G.F.Romanova, P.I.Didenko, V.A.Chernobai. Mikroelektronika, 22, No.3, 51 (1193).
30.E.F.Venger, S.I.Kirillova, V.E.Primachenko, V.A.Chernobai. Fizika i Tehnika Poluprovodnikov 29, (1995).
31.Yu.Lauke, Yu.M.Tairov, V.F.Tsvetkov, F.Shchepenski. Neorganicheskie Materiali, 17 254, (1981).
32.Yu.I.Gorkun. Fizika Tverdogo Tela, 3, 1061 (1961).
33.V.S.Vavilov, V.F.Kiselev, B.N.Mukashev. Defects in silicon

and on its surface. Moscow, 1990.

34 . L.A.Kosyachenko. Electroluminescence of a semiconductor diode under reverse bias. Sci.Proc. of the Tartu University, 1983, No.655, pp.12-33.

35.X.M.Altaiskii, V.K.Byalonovich, A.M.Genkin, V.S.Kiselev et al. High-stability silicon carbide LED. Pis'ma ZhTF, 1976, v.2, No.22, pp.1036-1037.

36.Yu.M.Altaiskii, S.F.Avramenko, A.M.Genkin, V.S.Kiselev. Wide-band LEDs with small area. Pribori i Tehnika Eksperimenta, 1986, No.2, p.245.

37.S.F.Avramenko, M.V.Belous, V.S.Kiselev. A small-size source of nanosecond light pulses. Pribori i Tehnika Eksperimenta, 1990, No.1, p.244.

38.A.E.Plaudis, G.K.Limezh, A.M.Genkin, V.S.Kiselev. A subnanosecond light pulse generator for determination of temporal characteristics of photodetectors. Technique and Equipment for physical investigations. Riga, 1989, pp.70-82.

39.S.F.Avramenko, V.S.Kiselev, A.N.Mahlin. An automated stand for measurements of the long-term stability of LED emission. Optoelektronika i Poluprovodnikovaya Tehnika. 1992, No.24, pp.54-57.

40.S.F.Avramenko, V.S.Kiselev. Avalanche Leds based on silicon carbide. Optoelektronika i Poluprovodnikovaya Tehnika. 1992, No.24, pp.57-61.

41.Violina G.I., Holuyanov T.F. Silicon carbide in thermal resistors and photodetectors.- Voprosi Radioelektroniki, ser. detali i komponenti apparaturi, 1965, No.4, 98-106

42.Campbell R. Silicon carbide junction thermistor - Silicon Carbide - 1973 - Univ. of South Carolina Press, p.611-617.

43.Wasa K., Tonda T., Kosahara Y., Hayakawa S. Highly reliable temperature sensor using RF-sputtered SiC-film -Rev.Sci.Instrum.- 1979, No.50, p.1084.

44.Nagai T. Yamamoto, Kobayashi I.- SiC thin film thermistor- J.Phys.E: Sci.Instrum.-1982, v.15, p.520-524.

45.S.F.Avramenko, V.S.Kiselev et al. - high temperature thermal resistors based on silicon carbide. Abstracts, VII Intern. Conf. "Electrical methods and means to measure temperature (T-92)", Lviv, Sept. 15-17/1992.

46.S.F.Avramenko, V.S.Kiselev, A.A.Pavlenko. A method of

fabrication of thermal resistors based on silicon carbide. A claim for Patent of the Ukraine. Priority date: Apr. 26/1993, No. 93121852.